Scientific report

regarding the implementation of the project PCE Ideas no. 342/2011
during the period December2014 – December2015

The present report structure follows the Work Plan proposed for the V-th stage of the project (Act Adițional 2/2015). Nearly all the reported results currently have been communicated at national and international conferences and published in ISI journals.

Phase objective: Characterization of the correlation between the delayed luminescence and mitochondrial metabolism

Characterization of the correlation between the delayed luminescence and mitochondrial metabolism

1. Introduction

Following previous researches, we have proposed ourselves to obtain new insights concerning the correlation between the delayed luminescence and the mitochondrial metabolism by using two flavonoids, epigallocatechine-3-gallate (EGCG) and quercetin (QC; 3,5,7,3',4'-pentahydroxyflavone), and the inhibitor of the mitochondrial respiration rotenone (ROT). EGCG and QC are two well-investigated flavonoids which inhibit cell proliferation and induce apoptosis in various cancer cell types [Johnson MK, Loo G. 2000, Han DW et al. 2011, Baran I., et al. 2010, 2012, Chen D et al. 2005, Jeong JH et al. 2009, Yen GC et al. 2003]. Both EGCG and QC can exert a dual, pro- and anti-oxidant effect, depending on dosage and time of treatment and numerous studies have indicated that malignant cells are more susceptible than normal cells to the cytotoxicity of these two flavonoids [Han DW et al. 2011, Chen D et al. 2005, Jeong JH et al. 2009, Yen GC et al. 2003]. Therefore, this property could be exploited to prevent leukemia or to increase the efficiency of leukemia chemotherapies. A clinically important chemotherapeutic agent used in the treatment of leukemia is menadione (vitamin K_3) (MD)[Matzno S et al. 2008], that produces important amounts of superoxide at the level of Complex I of the miochondrial respiratory chain (MRC)[Floreani M, Carpenedo F. 1992]. MD, H_2O_2, QC and EGCG can activate the apoptotic program via a Ca^{2+}-dependent mitochondrial pathway [Johnson MK, Loo G. 2000, Han DW et al. 2011, Baran I., et al. 2010, 2012, Chen D et al. 2005, Jeong JH et al. 2009, Yen GC et al. 2003, Matzno S et al. 2008, Floreani M, Carpenedo F. 1992, Barbouti A et al. 2007].

By continuing previous studies [Baran I., et al. 2010, 2012, 2013, various phases of this project], we have proposed ourselves to investigate into more detail the correlation between apoptosis, oxidativ stress and delayed luminescence, as well as its relationship with the mitochondrial metabolism. In order to induce the oxidative stress we have used menadione (MD) and hydrogen peroxide (H_2O_2), and the two flavonoids, quercetin and epigallocatechin-3-gallat, applied alone or in combination with MD or H_2O_2. In collaboration with our partners from LNS Catania, Italy, we endeavoured to contribute to a better undestanding of the biochemical mechanisms responsible for delayed luminescence of the living cells and, on the other hand, to obtain new data concerning the relationship between DL an the cell state. Our measurements had as objective the studiy of the effects of above mentioned agents on the human leukemia Jurkat T lymphoblats.

An active area of current research is represented by the studies aiming at finding methods for the early detection of malignant diseases, among them leukemia, in order to devise more efficient therapies against cancer. Delayed luminescence (DL) is one of these methods belonging to the group of optical techniques, considered to be mostly non-invasive and able to perform a rapid and inexpensive screening [Scordino, A. et al, 2014]. Delayed Luminescence (DL) is the photo-induced ultra-weak luminescence emitted by biological systems for long time after the illumination source has been switched off. This method could be an excellent candidate for developing a reliable and inexpensive optical biopsy technique [Scordino, A. et al, 2014]. Therefore, studies regarding the correlation between DL and the functional state of the living cell

could provide valuable information in order to discriminate between normal and malignant cells. Progresses achieved in the last years have shown that mitochondria play a key role into controlling life and death in addition to their established role in generating energy for the cell. Indeed, with a few exceptions, the mitochondria represent an essential component of many apoptotic pathways [S. Desagher and J-C. Martinou, 2000] by releasing cytochrome c into the cytosol and thereby activating caspases. In this respect, recent results of photoinduced delayed photon emission from leukemia Jurkat cells [Baran I., et al. 2010, 2012, 2013] supported the notion that DL is mainly produced within the mitochondrial electron transfer system at the level of Complex I. Therefore, we have propesed ourselves to get more insight into this topic and to elaborate a model of the DL generating states produced during the electron transfers at the level of the MRC Complex I.

2. Materials and methods

2.1. The delayed luminescence method. In order to understand the results of our measurements, it is necessary to describe the DL method and to show what kind of informations it could provide. Delayed Luminescence is a polyphasic signal, with a lifetime spectrum extending from about 10^{-7} s to more than 10 s. Due to its weakness (its intensity being $10^3 \div 10^5$ smaller than that of fluorescence), the signal is prone to noise contamination. Consequently, in order to record such a low level signal, a sensitive and reliable single-photon detection system has to be developed. Moreover, DL detection is still more difficult in the case of mammalian cells since the excitation spectrum shifts toward the high frequency region and it could occur that the DL spectrum overlaps the excitation spectrum of the materials commonly used as sample holders, typically plastic or quartz cuvette, in the standard equipment [C. Mieg et al., 1992]. In order to prevent such problems our partners from LNS-INFN Catania [Tudisco S.A. et al., 2003, 2004, Scordino et al., 2014] have designed and realized a new equipment taking into account some specific requirements: (i) the ability to detect single photon events, (ii) a very low background noise, (iii) high efficiency in the collection of the luminescence coming out from cell cultures, (iv) a short delay time between the end of the illumination pulse and the beginning of the acquisition, (v) low quantities of cells to be used. This system, called ARETUSA "**A**dvanced **R**esearch **E**quipment for fas**T** **U**ltraweak lumine**S**cence **A**nalysis" [Tudisco S.A. et al., 2003, 2004] has been used for recording the delayed luminescence of cell cultures. This system can detect single photon events and the background noise is very low, as it was required. At the same time, the efficiency in the light collected from the cell cultures was very good and the signal recording starts with a very short delay after the illumination pulse was over. A schematic drawing of the set-up is represented in Fig. 1. The detector is a photomultiplier tube (PMT) Hamamatsu R-7206-1 (multialkali, spectral response 300-850 nm), selected for single photon counting. The excitation source was a pulsed nitrogen laser (Laserphotonic LN203C) providing pulses at λ=337 nm, and a pulse duration of 5 ns, with an energy of 100±5 μJ/puls. During the measurements the laser intensity should be under constant control. To this aim an extremity of the optical fiber used for illumination was connected to a standard energy-measuring head (Power Meter Ophir PE10-V2). The error due to the laser intensity fluctuations is about 3-4%. In order to prevent the damages coming from the large quantity of photons diffused by the sample during the laser pulse, an electronic shutter turned off the PMT detector. Thus DL emission was observed in a dynamic window starting from about 10 μs and lasting until the signal is well above the background. The detected DL signals were recorded via computer through a multi-channel scaler (Ortec MCS PCI) plug-in card, which can collect analogical or logical signals into a defined temporal window as a function of time. In order to reduce the random noise a smoothing procedure was used: the experimental points were sampled in such a way that it was $\Delta t_i/t_i$ constant, so that data resulted equally spaced over a logarithmic time axis [Scordino A. et al., 1996, 2014].

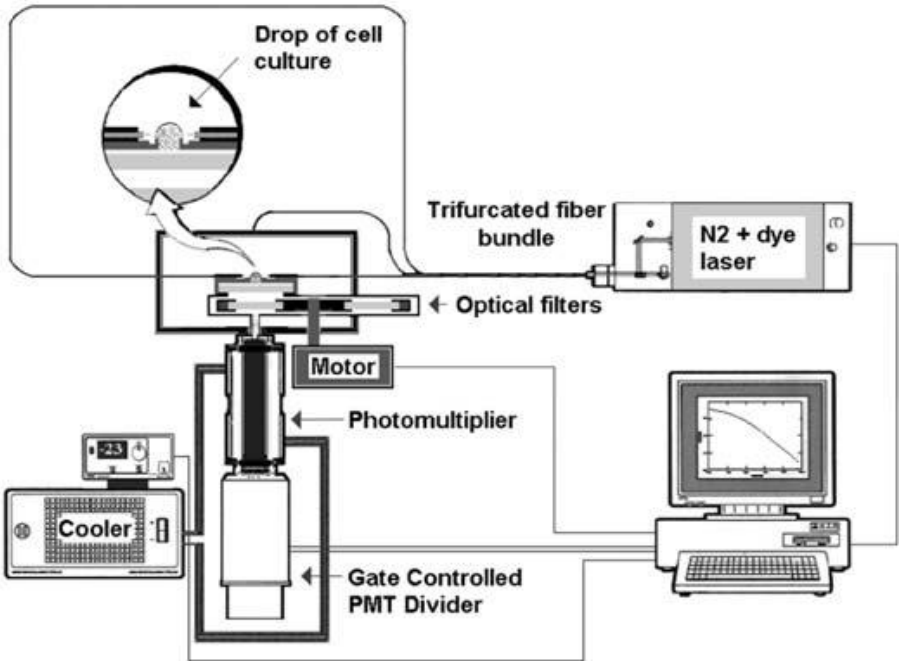

Fig.1. The ARETUSA experimental set-up [Scordino A. et al., 2014]

Generally, the low emitted intensity of the DL signal did not allow getting high spectral resolution. Therefore, for spectral analysis a set of broadband (80 nm FWHM) Thermo-Oriel interference filters were placed between the sample and the photomultiplier. To reduce significantly the background noise, the photomultiplier was cooled down to -30°C using a circulating cold liquid in direct contact with its surface. The detector has been placed as close as possible to the sample, so that, from point of view of the geometry, the total efficiency of this type of arrangement is about 8%, i.e. an order of magnitude higher than that obtained with previously used systems. [Scordino A. et al., 2014]. The most important source of background in these measurements was represented by the DL emitted by parts of the set-up itself, as for instance the sample holder, if reached by even a fraction of the excitation light. Thus, in order to avoid the use of any holder for the sample, DL measurements on cell cultures were performed placing a volume of about 150 μL of the cells suspension (one drop) directly on the quartz window (diameter 5 mm) of a liquid light guide (Edmund Optics NT53-694), transmitting more than 40% of the impinging light in the interval between 300 and 700 nm. At the opposite end, the light guide was connected straight to the photocathode by a small quantity of optical gel. The apparatus was enclosed in a dark chamber, made of plastic material characterized by very low luminescent emission, and coated on the inner surface with a special low luminescent paint. From a geometrical point of view the total efficiency of such an arrangement was about 10%. In order to guarantee a uniform illumination of the sample drop, the laser was connected to an optical fiber having the output end divided into three parts, which were arranged around the drop at constant angles of 120° among them. Nevertheless, some background noise came from the quartz window of the liquid light guide. Indeed, the sample drop, acting like a hemispherical lens, excites the quartz window projecting 20% of the total laser on it. In order to discriminate DL generated in the sample from background noise relatively high cell densities were needed. With the double aim to reduce the necessary sample quantity and to limit possible unwanted background signals arising from excitation of part of the set-up, a novel sample holder was designed and realized [Scordino A. et al., 2008, 2014]. It consists from a hollow cylinder having at the top a closure disc with a small hole 3.5 mm in diameter. The sample consists of a small liquid lamella (volume = 20÷25μL) with the cells suspended in it, sustained only by contact with the border of the circular hole, so

avoiding the presence of any solid material behind it. This configuration presented many advantages with respect to the previous one. Indeed, smaller quantities of sample were necessary to perform measurements. Moreover, the geometry of the set-up avoided unwanted background signals coming out from any solid material underlying liquid sample. Finally, the closure disc of the sample holder could be changed from one sample measurement to the other one, so avoiding problems of contamination. Such improvement experimental set-up was used in the study of DL from leukemia Jurkat cells [Baran I. et al., 2010, 2012, 2013, Scordino A., et al., 2014].

2.2. Cell cultures. Human leukemia Jurkat T-cell lymphoblasts were cultured in suspension in MegaCell RPMI 1640 medium supplemented with 5% heat-inactivated fetal bovine serum, 2 mM L-glutamine, 100 units/ml penicillin and 100 μg/ml streptomycin, at 37ºC in a humidified incubator with a 5% CO_2 atmosphere. Exponentially growing cells were adjusted to a density of 0.2×10^6 cells/ml the day before the experiment. We used hydrogen peroxide 30% solution and stock solutions of menadione sodium bisulphite dissolved in phosphate buffer saline (PBS), or dihydrated quercetin and epigallocatehin gallate dissolved in dimethyl sulfoxide (DMSO). In combined treatments, the oxidant agent was added directly to the cell cultures after preincubation with QC or EGCG as specified, without intermediary wash out. The rotenone was dissolved in DMSO. DMSO was 0.125% (v/v) in all cell cultures. Unless specified otherwise, all chemicals were from Sigma-Aldrich. After each treatment, cells were washed thoroughly with PBS and resuspended in PBS (for DL samples, $\sim 40 \times 10^6$ cells/ml) or in complete medium for apoptosis assessment ($\sim 0.2 \times 10^6$ cells/ml). DL and fluorometric samples were analyzed immediately by DL and fluorescence spectroscopy. Cell density, viability and morphology were examined with a CCD camera Logitech QuickCam Pro 4000, connected to an Olympus CK30 phase contrast microscope. For cell density assessment, 25 μl- aliquots of the DL samples were diluted in PBS, stained with 0.4% trypan blue solution and ~1500-2000 cells were imaged on a Bürker haemocytometer at the time of the DL assay. Cell count evaluation was performed both during DL experiments, directly by visual inspection under the microscope, and later on, by analyzing the micrographs with the use of the software ImageJ.

2.3. Delayed luminescence spectroscopy measurements. For the measurements we have used the improved version of the ARETUSA system described above. The detected signals were acquired by a Multi-channel Scaler (Ortec MCS PCI) with a minimum dwell-time of 200 ns. DL measurements were done on at least 3 different drops from each cell sample (drop volume 15-25 μl) at room temperature (20 ± 1ºC). PBS luminescence was subtracted from all recordings. Photoemission was recorded between 11 μs and 100 ms after laser-excitation. DL intensity (*I*) was obtained as the number of photons recorded within a certain time interval divided to that time interval and to the number of living cells in the drop. The quantum yield was calculated in three time-domains of the DL emission: 11-100 μs (DL-I), 100 μs - 1 ms (DL-II) and 1-10 ms (DL-III), as the ratio between the *I*-integral and the energy of the laser. This analysis could not be performed in consistent manner in the time domain 10-100 ms, as in some cases the signal-to-noise ratio was too high within this region. The intensity of Yellow/Green DL was estimated by subtracting the additive contribution of Blue and Red DL intensities from the VIS DL intensity. The time decay data of DL photoemission curves were fitted with an equation of the type: $y = = \sum A_i \exp(-t/\tau_i)$ having a variable number of exponential components. For each set of VIS, Blue, Green/Yellow or Red DL emission data, the time decay constants (τ_i) and the minimal number of exponential DL components were established from the best simultaneous fit to all DL curves obtained with control- and rotenone-treated cells in the respective spectral data set. Then the DL yield corresponding to each kinetic component was calculated for each individual DL curve as the product $A_i \tau_i$. To facilitate comparison between different spectral DL components, the DL yield was calculated in some cases in three time domains of the DL emission, corresponding to three main classes of light emitting states: 11-100 μs (S_1 states), 100 μs - 1 ms (S_2) and 1-10 ms (S_3), as the

integral of the *I*-fitting function over the respective time domains. This analysis could not be performed in a consistent manner in the time domain 10-100 ms, as in some cases the signal-to-noise ratio was too high within this region.

2.4. Statistics. Unless indicated otherwise, the data are presented as median ± s.e.m. of at least three different measurements. ***For data fit*** we have used the Origin software, version 7.5.

3. Results

3.1. Determination of DL characteristic values (kinetics, quantum yield, spectral components) in EGCG treated cells

In a first stage we have studied the characteristic features of delayed luminescence following the treatments of Jurkat cells with EGCG at various concentrations. In contrast with quercetin, EGCG exerted a qualitatively different effect on DL by producing a fairly uniform reduction of the photoemission intensity along the entire timescale. (Fig. 2). EGCG acted as an antioxidant against the DL-II reduction by H_2O_2 treatment.

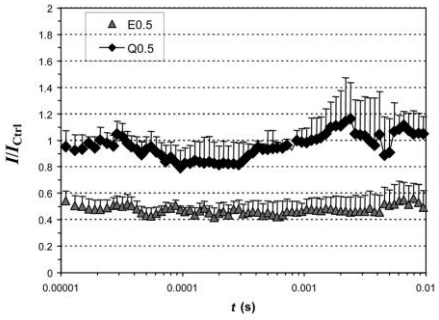

Fig. 2. The kinetics of DL emission of Jurkat cells after treatments with flavonoids. The treatments are marked in the figure. The light intensity of the treated cells (*I*) was normalized to the DL intensity of the control cells (I_{Ctrl}).

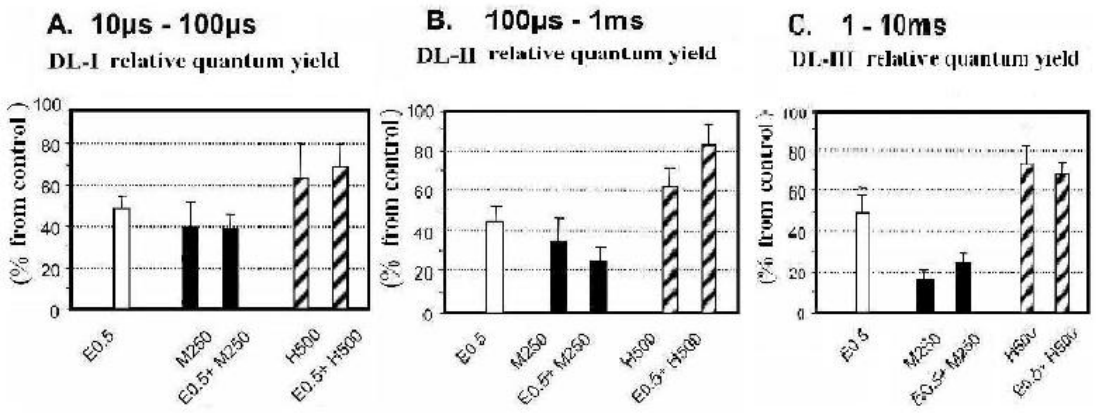

Fig. 3. Quantum yield of DL as compared to the control (**A**-**C**) for various treatments as indicated in the figure. E, M/ME, H/ HE represent treatments with EGCG, treatments with MD with and without pre-incubation with EGCG, treatments with H_2O_2 with and without pre-incubation with EGCG. The results obtained for DL time domains are individually presented for DL-I (**A**), DL-II (**B**) and DL-III (**C**).

Thus, the pre-treatment with 10 μM EGCG for 24 h was able to induce a significant recovery of DL-II emission. Also, in the case of drastic DL reduction following treatment with menadione, pre-incubation with EGCG generally induced partial recovery of DL-III up to ~25% of the resting value. Fig. 3 depicts the relative values of quantum yield in the three domains of DL emission after EGCG treatments and combined treatments with menadione and hydrogen peroxide. Regarding the spectral component, we have found a uniform effect of EGCG for all the studied wavelengths and therefore not shown.

3.2. Determination of the dependence/independence of delayed luminescence of the mitochondrial membrane potential and of the mitochondrial superoxide level

Our previous studies have indicated that DL is correlated with the activity of the Complex I of the mitochondrial respiratory chain (MRC) but not with the existence of DNA strand breaks [Baran I. et al, 2009, 2010]. We have found previously that menadione (MD), quercetin and hydrogen peroxide can act as inhibitors of DL [Baran I. et al, 2010].

We have continued our investigations regarding the correlation between the mitochondrial metabolism and DL by using again the inhibitor of the mitochondrial respiration rotenone (ROT). As we have previously mentioned (report 2013) the specific inhibitor of mitochondrial respiration ROT [Li N., 2003, Xu X., E.A. Arriaga, 2009], binds to two specific distinct non-interacting sites on Complex I of the mitochondrial respiratory chain (MRC) [Suzuki H., T.E. King, 1983, Grivennikova V.G. et al., 1997]. These ROT sites, denoted as ROT site 1 and ROT site 2, are most likely situated in the 49-kDa and ND1 subunits of Complex I, respectively [Albracht S.P.J. et al., 2011]. ROT site 1 and ROT site 2, which display different affinities for the inhibitor [Magnitsky S. et al., 2002], appear to be involved in the forward and reverse electron transfer, respectively [Grivennikova V.G. et al., 1997]. It is widely accepted that in the forward mode (site 1 involved) rotenone disrupts the electron flow at the level of protein-bound ubiquinone adjacent to center N2 (Q_{Nf}), specifically by destabilizing the ubisemiquinone produced after acceptance of the first electron from center N2 [Ohnishi S.T. et al., 2005]. As a direct consequence of the rotenone blockage, respiration ceases and the intracellular level of NADH augments due to lack of consumption by the mitochondria. Moreover, the accumulating electrons are deviated from Complex I to the surrounding molecular oxygen, thereby producing superoxide ($O_2^{-\bullet}$) at elevated rates, which is then released into the matrix [Xu X., E.A. Arriaga, 2009]. The superoxide produced by the mitochondrial electron transport chain is rapidly converted to hydrogen peroxide (H_2O_2) by the action of mitochondrial superoxide dismutases. Rotenone and rotenoids in general have demonstrated anticancer activity which was attributed to the induction of apoptosis [Isenberg, J.S. , J.E. Klaunig, 2000, Li N. et al., 2003]. The apoptotic effects of rotenone on human leukemia Jurkat T cells have been reported in several studies involving particular doses and application times [Isenberg, J.S. , J.E. Klaunig, 2000, Yin W. et al., 2009].

Our previous studies [Baran I. et al., 2014] concerning the determination of rotenone effects on the Jurkat cells, by means of spectrofluorimetry, have evidenced modifications of mitochondrial superoxide level and that of intracellular NADH. A consistent increase of both species was displayed after addition of rotenone, with a maximum after ca. 40-60 min., followed by a period of marked decrease of the superoxide level (Fig. 4, 5). Since both MD and QC inhibit the mitochondrial

respiration at Complex I, we have investigated into more detail the mechanisms by which these compounds have an effect on DL which opposes to that of ROT..

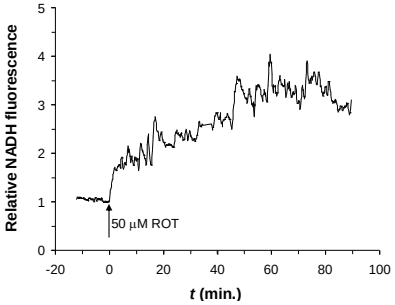

Fig. 4. Time course of the variation of intracellular NADH relative level in Jurkat cells suspensions before and after exposure to 50 μM rotenon [Baran I. et al., 2014].

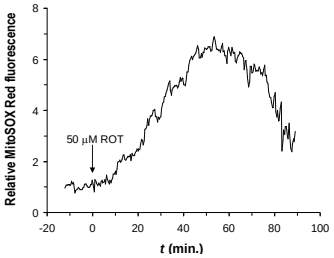

Fig. 5. Time course of the variation of superoxide relative level in Jurkat cells suspensions before and after exposure to 50 μM rotenon. The value of the fluorescence intensity of the MitoSOX Red indicator has been taken having as reference the average value recorded during a period of 10 min. before the addition of ROT in the suspension [Baran I. et al., 2014].

With this aim we have measured the intracellular NADH and mitochondrial superoxide levels variations after exposure to different doses of ROT. As expected, both level have increased consistently (up to ~8 times) (Fig. 6). On the contrary QC decreased substantially (about ~3-5 times) both the levels of NADH and that of superoxide, probably exerting an antioxidant effect which prevented the accumulation of these species) (not shown).

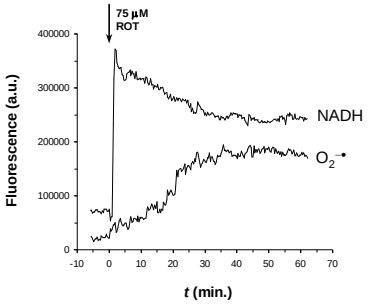

Fig. 6. Time course of NADH and mitochondrial superoxide levels in suspensions of Jurkat cells exposed to 75 μM ROT.

Importantly, our measurements have indicated for the first time a very strong correlation between the DL quantum yield and the level of cellular NADH and mitochondrial superoxide (Fig. 7), which was characterized by a Pearson correlation coefficient of 0.95 and 0.96 (in the visible domain), and 0.84 and 0.88

(at 686 nm), respectively. Taken together, these data provide strong evidence supporting the idea that Complex I of the mitochondrial respiratory chain is an important source for delayed luminescence in living cells, and suggest that DL is quantitatively correlated with the level of both NADH and mitochondrial superoxide. In addition, our measurements indicate that charge recombination at the N2 center of Complex I produces delayed luminescence with a characteristic wavelength of 686 nm and a decay time constant of 132 μs.

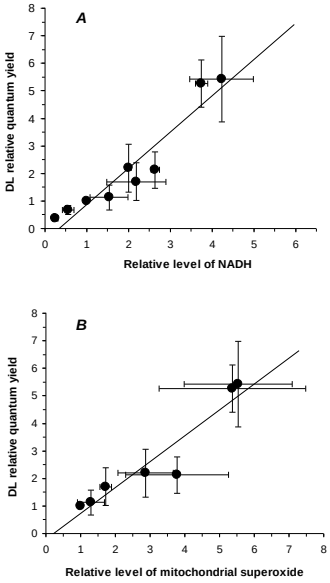

Fig. 7. Correlation between the DL relative quantum yield in the visible domain and the level of NADH (***A***) and mitochondrial superoxide (***B***) relative to the control.

Further, we have tried to quantify the effects of ROT on delayed luminescence of Jurkat lymphoblasts. Our studies [Baran I. et al., 2013] suggested that the redox processes at the level of Fe/S centers, that are occuring during the electron transfers in the Complex I of the mitochondrial respiratory chain, have a dominant contribution on a time scale of 10 μs - 10 ms.

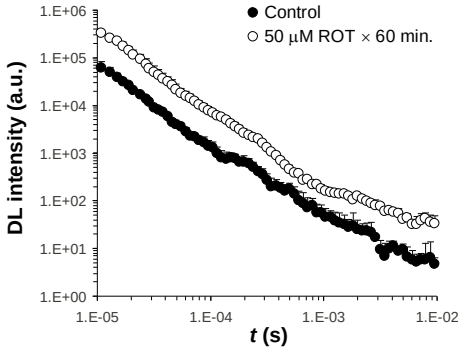

Fig. 8. Time course of DL emission in non treated cells suspensions (Control) or treated with 50 μM rotenon for 60 min.

In order to evaluate the DL characteristics, the cellular samples, both untreated and treated with 50 μM ROT, have been washed twice with PBS and resuspended in

PBS at a concentration of 30×10^6 cells/ml and have been illuminated with a pulsed UV radiation from a nitrogen source with the characteristic wavelength of $\lambda = 337$ nm. The photon emission of the sample in the visible domain (VIS) was measured in the interval of 11 μs – 10 ms from illumination, by DL spectroscopy, using the photomultiplier tube Hamamatsu R-7602-1/Q. We have calculated the quantum yield in three domains of the DL emission, respectively: 11 - 100 μs (DL-I), 100 μs - 1 ms (DL-II) and 1 - 10 ms (DL-III), as the ratio between the *I*-integral (*I* the intensity of the laser beam as a function of time) and the energy of the laser. At 50 μM ROT we have obtained a biphasic dependence on the treatment time, exhibiting a maximum in VIS at 60 min. and a significant recovery for treatments of 90 min. (Fig. 9). We have recorded a substantial increase of the quantum yield in all three domains for the samples treated with 50 μM ROT for 60 min., as compared with the control (untreated ones) with (Fig. 9).

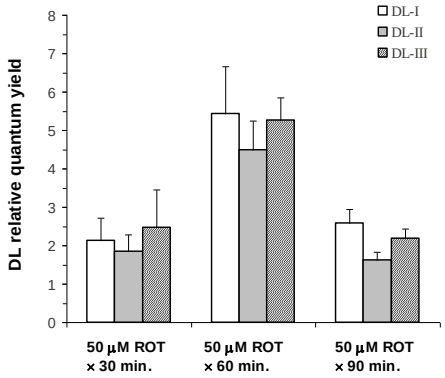

Fig. 9. Relative quantum yield of DL emission in VIS in cells suspensions treated with 50 μM rotenon for 30, 60 or 90 min. The quantum yield calculated for the three time domains was taken in reference to the corresponding value obtained for non treated cell suspensions.

These results have been correlated with the preferential induction of apoptosis, not necrosis after treatments with rotenone in this cellular system. The photon emission of the sample was recorded at $\lambda = 686$ nm in the time interval of 11 μs - 10 ms after illumination by DL spectroscopy, using an interferential filter Lot-Oriel having a bandwidth of 80 nm for the selection of the transmitted light wavelength (Fig. 10).

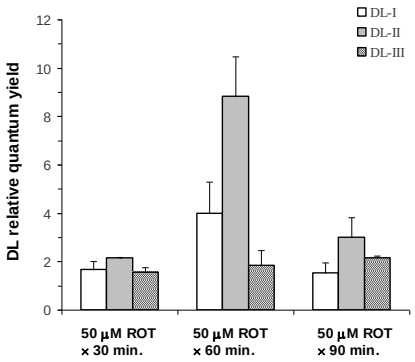

Fig. 10. Relative quantum yield of DL emission at 686 nm in Jurkat cells suspensions treated with 50 μM rotenon for 30, 60 or 90 min. The quantum yield calculated for the three time domains was taken in reference to the corresponding value obtained for non treated cell suspensions.

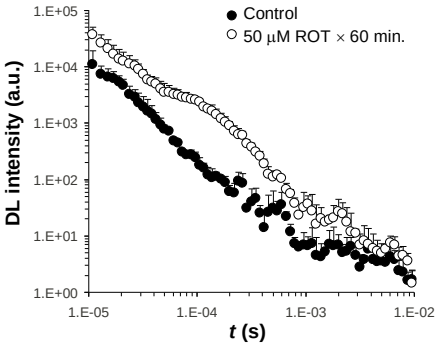

Fig. 11. Kinetics of DL emission at 686 nm in non treated Jurkat cell suspensions (Control) or treated for 60 min. with 50 μM ROT.

At this dose of ROT, have obtained a biphasic dependence on the treatment time, exhibiting a maximum at 60 min. at 686 nm and a significant recovery for treatments of 90 min. (Fig. 10). The DL-II component presented a marked variation as compared with -I and DL-III. From the fit of the kinetic data of DL emission (Fig. 11) we have obtained a characteristic time constant of 132 μs, as previously shown, that can be interpreted as being correlated with the redox reactions taking place at the level of the N2 redox center of the mitochondrial respiratory chain Complex I.

Further, we have studied the dependence of DL on the ROT dosis in Jurkat lymphoblasts. The cellular suspensions have been incubated, being or not exposed to 25 μM, 50 μM and 75 μM ROT, respectively, for 30 min. at 37ºC. DL samples have been then prepared in PBS at a concentration of 30×10^6 cells/ml and illuminated with pulsed UV radiation (λ = 337 nm). The photon emission of the sample was measured on the entire visible domain (VIS) and also at the wavelengths of 460 ± 40 nm and 686 ± 40 nm, respectively, in the time interval 11 μs - 20 ms. Each experiment was performed in triplicate, realizing thus a total number of 24 measurements, including the non-treated cell samples. For each dose of ROT we have calculated the mean values of the DL photoemission intensity as a function of time and we have fitted each emission curve with a sum of 4 exponentials (in VIS) or 6 exponentials (for the emission at 460 nm or 686 nm).

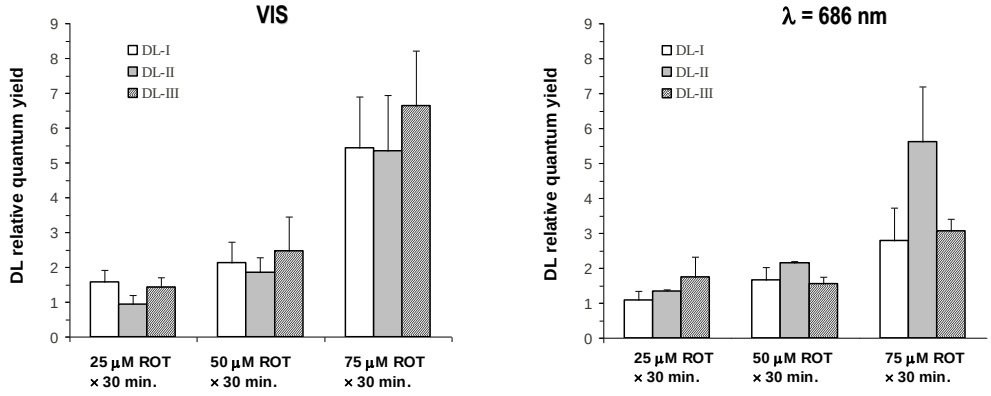

Fig. 12. Relative quantum yield of DL emission in VIS or at 686 nm in cells suspensions treated with 25, 50 or 75 μM rotenon for 30 min. The quantul yield calculated for the three time domains was taken in reference to the corresponding value obtained for non treated cell suspensions.

The resulted characteristic time constants were: 22.9 μs, 140 μs, 1.40 ms and 8.50 ms (in VIS), respectively 13.3 μs, 129 μs, 388 μs, 1.70 ms, 3.87 ms and 8.25 ms for red (at ~686 nm) or blue (at ~460 nm) light emission.These values give indications about the different rates of electronic transfer al the level of Complex I of the mitochondrial respiratory chain. We have recorded an increase of the quantum yield with the rotenone dose in all three DL domains as compared with the non treated samples, as follows (Fig. 12): 1) in VIS, for 25 μM ROT, the average increase was of 1.5 times for DL-I, of 1.1 times for DL-II and of 1.3 times for DL-III, respectively, and at 50 μM ROT, the average increase was of 2.1 times for DL-I, of 1.9 times for DL-II and of 2.6 times for DL-III, respectively; 2) at 686 nm, for 25 μM ROT, the average increase was of 1.2 times for DL-I, of 1.3 times for DL-II and of 1.7 times for DL-III, respectively and at 50 μM ROT, the average increase was 1.6 times for DL-I, 2.1 times for DL-II and 1.4 times for DL-III, respectively.

ROT elicited strong effects on the delayed luminescence (Fig. 12). After treatments with 75 μM ROT for 30 min. the quantum yield of DL in the visible domain has increased ~6-times. Interestingly, the time dependence of the ROT effect on Dl was biphasic, with an observed maximum for treatments of 60 min. duration, followed by a substantial recovery at 90 min., indicating that the cells have neutralized the blocage induced by rotenone. This idea is also strongly supported by the observed absence of necrosis, suggesting that the cell have resumed the mitochondrial respiration. The DL amplification observed for the optimum treatment duration (60 min.) increased as the rotenone dose increased. Similar effects have been observed when DL was recorded at λ = 686 nm, while at λ = 460 nm there was not any measurable difference as compared to control (not shown). At λ = 686 nm DL presented a marked increase in the DL-II domain and the photoemission kinetics has shown a distinct exponential component with a time constant of 132 μs. This value is in good agreement with the rate of electron transfer at the two extreme Fe/S centers N1a and N2 in the Complexul I of MRC [Fiorani M. et al., 2010], suggesting that DL-II/686 nm could be good measure of the electron transfers at the level of N2 center, the closest to the ubiquinone site in Complex I.

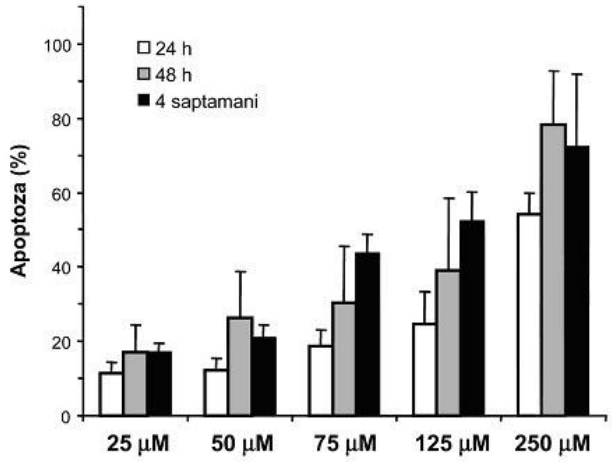

Fig. 13: Rotenone induces apoptosis in Jurkat cells in a dose-dependent manner. Apoptosis was evaluated 24 h and 48 h after treatment with ROT for 1 h at indicated doses. In the figure it is represented the death rate calculated from the clonogenic survival obtained 4 weeks after treatment (black bars) compared to the rate of apoptosis (white/grey bars) obtained after subtracting the nonspecific apoptotic rate.

Rotenone induces apoptosis in Jurkat cells in a dose-dependent manner (Fig. 13). Our results are in agreement with previous data (report 2013) and are evidencing the tight correlation between the mitochondrial metabolism and delayed luminescence. These data are completed with those regarding the mitochondrial level of NADH and FMN, which will be presented in the following chapter.

3.3. Characterization of the correlation between the delayed luminescence and the mitochondrial level of NADH and FMN after a large series of treatments with quercetin, menadione, rotenone and EGCG.

By means of DL we have monitored the effects of MD, H_2O_2, QC, and EGCG on apoptosis and cell cycle in human leukemia Jurkat cells. The characteristic growth of Jurkat cells in suspension made this cell type more suitable for DL investigation, as it greatly minimized the sample preparation time and the cell stress during probation for delayed luminescence, and any artifactual interference of a supplementary trypsinization step with the cellular metabolism was thus avoided.

Menadione (vitamin K3) is a clinically important chemotherapeutic agent used in the treatment of leukemia and other cancer types. MD participates in redox cycling reactions catalyzed by a number of flavoenzymes, thus producing intracellularly large amounts of superoxide anion. Menadione reduction at Complex I of the mitochondrial respiratory chain (MRC), which accounts for 50% of menadione metabolism, can readily divert the electron flow from Complex I and therefore interfere with mitochondrial respiration. Quercetin (QC) is a natural flavonoid that can display both antioxidant and pro-oxidant properties. The employment of quercetin-combined treatments has been proposed to increase the efficiency of leukemia chemotherapies. Moreover we took advantage of the specific ability of quercetin to accumulate inside the mitochondria of Jurkat cells, as well as of the fact that both quercetin and menadione appear to interact robustly with the mitochondria and to induce apoptosis through the mitochondrial pathway. Thus, we could probe whether DL is connected to the mitochondrial metabolism.

Different concentrations and incubation times of menadione, hydrogen peroxide, quercetin and epigallocatechin gallate, as well as combined treatments, were tested by evaluating, via flow-cytometry, cell fractions in each cell cycle phases. Apoptosis was evaluated as the fraction of hypodiploid cell fragments (the sub-G_0/G_1 cell fraction). More precisely, Jurkat cells were treated with 0.5, 5, 50 μM quercetin for 24 h, 10 or 50 μM quercetin for 1 h, 25 μM menadione for 20 min and 4 h, 250 μM menadione for 20 min, 100 or 500 μM hydrogen peroxide for 20 min, 0.5 μM epigallocatechin gallate for 24h, and combined treatments of QC or EGCG pre-incubation followed by addition of 250 μM menadione or 100/500 μM H_2O_2 for 20 min. We have performed the DL measurements for the above mentioned treatments.

DL intensity *I* was normalized to the number of living cells in the sample. The DL curves of Jurkat cells presented a complex, multi-component decay. To better evidence the effects of various chemical treatments on DL kinetics, we also represented the time course of the photoemission intensity relative to the DL intensity of control cells, as it is reported in Fig. 14.

This depiction revealed that there are three distinct time domains in which DL manifests different characteristics, namely 11 - 100 μs (denoted DL-I), 100 μs - 1 ms (DL-II) and 1 - 10 ms (DL-III). At increasing doses, quercetin inhibited DL progressively [Baran I. et al., 2010, 2012, Scordino A. et al., 2014]. The most sensitive DL region was DL-III, which decreased by one order of magnitude after the

treatment with 50 μM QC for 24 h, whereas DL-I was only slightly affected by QC. EGCG exerted a qualitatively different effect on DL by producing a fairly uniform reduction of the photoemission intensity along the entire timescale. 500 μM H_2O_2 applied for 20 min. reduced DL significantly over the regions DL-I and DL-II.

Pretreatment with 0.5 μM EGCG for 24 h was able to induce a significant recovery of DL-II emission, whereas preincubation with 10 μM QC for 1 h further reduced the DL-III intensity. The lower dose of 100 μM H_2O_2 had a modest effect on DL and inhibited photoemission by ≈22% over the entire timescale. Preincubation with 50 μM QC for 24 h restored DL-I emission but inhibited substantially DL-II and DL-III. Menadione also inhibited DL in a dose-dependent manner. In addition, at variance with the modest effect of QC on DL-I, MD reduced substantially photoemission in the DL-I region.

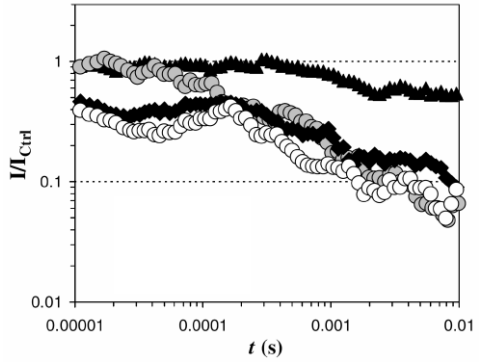

Fig. 14. Kinetics of DL emission from Jurkat cells at various treatments: 5 μM (▲) and 50 μM (grey circles) QC for 24 h, 250 μM menadione for 20 min, alone (◆) and after (○) preincubation with 5 μM QC for 24 h. The intensity of the light emission (I) is normalized to the DL intensity of untreated culture (I_{Crl}).

This inhibition was strong even at the lowest dose of 25 μM menadione. DL-II was inhibited to a similar extent by high doses of MD, whereas DL-III exhibited a drastic reduction. Preincubation with the two flavonoids generally induced partial recovery of DL-III up to ~25% of the resting value, except in the case of pretreatment with 5 μM QC for 24 h, when a further reduction to 9.2 ± 3.8% was recorded. Moreover by evaluating the quantum yield, calculated in the three time-domains of the DL intensity curve as the ratio between the I-integral (in the considered time interval) and the energy of the laser, there is a significant (r = −0.63) negative correlation between DL-II and the apoptotic cell fraction with treatments of varying time and dosage of the two oxidative stress inducers, MD and H_2O_2, and two flavonoids, QC and EGCG. Furthermore, by selecting only treatments with MD, QC, and combinations of the two, we obtained a very strong anticorrelation (see Fig. 15) between both DL-II and DL-III quantum yield and apoptosis (r = −0.90 and −0.84, respectively).

All the set of data was consistent with the hypothesis that delayed luminescence from Jurkat cells originates in major part from Complex I of the mitochondrial respiratory chain (MRC). In Complex I, the two electrons delivered by reduced nicotinamide adenine dinucleotide (NADH) to flavine mononucleotide (FMN) are transferred between eight consecutive iron-sulfur clusters, eventually reaching the ubiquinone. Our findings suggested that upon UV irradiation, FMN can produce excited singlet states that may either decay to the ground state by prompt

fluorescence or undergo intersystem crossing to long-lived triplet states which can subsequently relax to some metastable intermediate states.

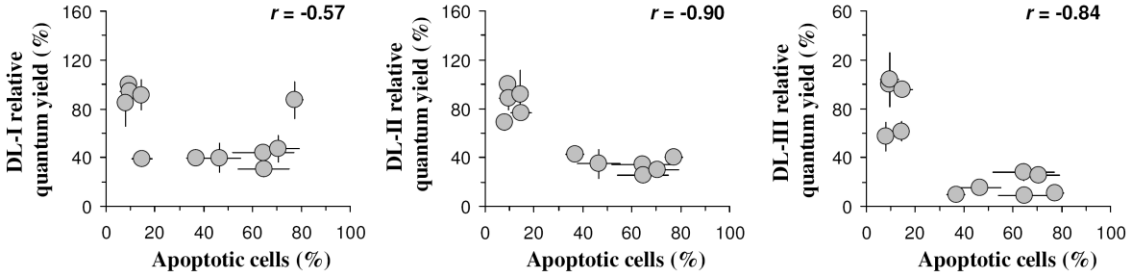

Fig.15**.** Relative DL quantum yield as a function of the apoptotic cell fraction for QC treatments and MD treatments with and without QC preincubation, in the three time interval of DL decay curve: 11 - 100 μs (DL-I), 100 μs - 1 ms (DL-II) și 1 - 10 ms (DL-III).

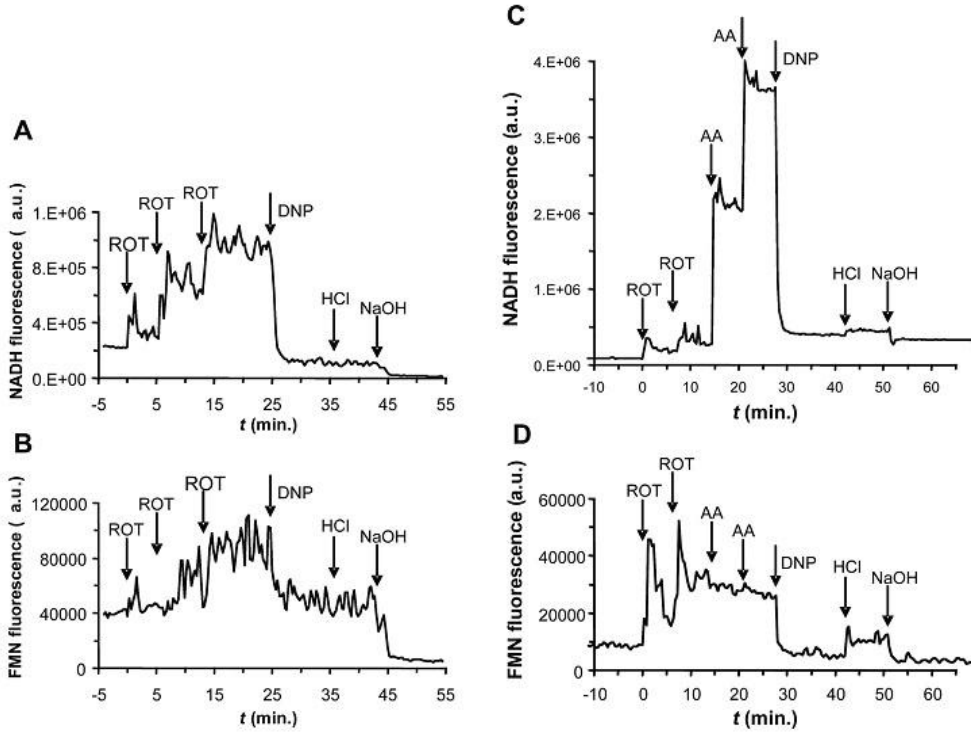

Fig. 16. NADH and FMN autofluorescence in Jurkat cells depend on the metabolic state of mitochondria. Kinetic traces of NADH (A) and FMN (B) autofluorescence in stirred suspensions of Jurkat cells on 37°C exposure to ROT and 2,4-dinitrophenol (DNP). At indicated time points (arrows), drugs were added in the sequence: three steps of 50 μM ROT each, then 75 μM DNP, and finally 2.5 mM HCl and 5 mM NaOH. Kinetic traces of NADH (C) and FMN (D) autofluorescence in stirred suspensions of Jurkat cells on 37°C exposure to ROT, AA, and DNP. At indicated time points (arrows) drugs were added in sequence: 50 μM ROT, 25 μM ROT, 4 μM AA, 4 μM AA, 75 μM DNP, 1 mM HCl, and 2 mM NaOH. The final pH was 6.9 and 7.6 after addition of HCl and NaOH respectively. The traces are representatives for three different experiments.

These triplet- or metastable-state species exhibit an intrinsically long lifetime, allowing a series of photochemical reactions to occur in Complex I via charge

recombination in the Fe/S redox centers and then produce secondary excitations, hence giving rise to delayed luminescence. It is worth to note that in Literature it is known that some electron transport inhibitors can affect light emission from chloroplasts [Felker P. et al, 1973] and Photosystem II, the first component in the photosynthetic electron transfer chain, represents the counterpart of MRC Complex I. Accordingly, our early data [Baran I. et al., 2010, 2012, Scordino A. et al., 2014] suggested that DL-I may be determined mainly by forward electron transfer reactions, whereas DL-II and DL-III may be determined by reverse electron transfer reactions within Complex I. Subsequent investigations [Baran I., et al., 2013] provided more detailed insights into the relationship between various DL characteristic times and the specific kinetic steps in the redox reactions that take place between NADH, FMN, the Fe/S centres and ubiquinone in respiratory Complex I, and delineated the main electron transfer pathways that could be associated with DL-I, DL-II and DL-III. The idea that mitochondrial Complex I plays a major role in the ultra-weak photon-induced delayed photoemission in Jurkat cells is reinforced by recent results [Baran I. et al., 2013] obtained by comparing the effects of MD and QC with those induced by Rotenone (ROT), a familiar specific inhibitor of mitochondrial respiration [Li N. et al., 2003], which is known to bind to two distinct, non-interacting sites on Complex I.

The results allowed also to elucidate the effect of quercetin on the activity of Complex I. The spectrofluorimetric determination of mitochondrial NADH levels, supported the idea that ROT inhibits, whereas QC, as MD too, stimulates Complex I activity by inhibiting or stimulating the dissociation of NAD+, respectively. These difference reflected also on the DL yield, both in the whole emission wavelength range and in the blue (λ_{em} = 460 nm) and red (λ_{em} = 645 nm) spectral components, as it is shown in Table I, where the effects of treatments that yielded about the same clonogenic survival are compared. The link of the DL to the mitochondrial NADH level is evident.

Table I. Relative levels of NADH and DL yield in leukemia Jurkat cells exposed to ROT and QC treatments with about the same clonogenical survival.

Treatment	**relative $[NADH]_m$**	**DL yield (VIS) 400-800 nm**	**DL yield (blue) 460 nm**	**DL yield (red) 645 nm**
Control	1	1	1	1
50 μM ROT × 30 min.	1,74	2,00	2,38	1,51
50 μM QC × 24 h	0,27	0,57	0,80	0,42

According to DL data, the blue light emission is most likely related to excited states of NADH, while the increased level of the red light after ROT treatments, taking into account the link to Complex I, is most likely produced via dimol photoemission (λ_{em} = 579, 634, and 703 nm) [Khan A. U., M. Kasha, 1970] generated by two colliding molecules of singlet oxygen ($^1O_2$). In regards to such point it must be noted that the broadband (80nm FWHM) filters used do not allow to univocally assign

the emission spectra. As a consequence, while when comparing normal versus tumor cells, the red component of DL emission could be attribute to protoporphyrin, in accord to autofluorescence measurements [Croce A. C. et al., 2011], when comparing leukemia (tumor) cells after ROT treatments our results differed from others [Mik E. G. et al., 2006, 2008] that reported a decrease of Protoporphyrin IX emission after ROT inhibition of mitochondrial respiration. The observed strong enhancement of the red DL components leads to the conclusion that, at least in Jurkat leukemia cells upon excitation at 337 nm, singlet oxygen is the dominant generator of red DL emission.

As a consequence, the timescales of various electron transfer steps involving the formation of flavin and ubisemiquinone radicals with subsequent production of superoxide can be estimated from delayed red-light emission. All these findings raise the attractive possibility that DL spectroscopy could be used as a reliable, sensitive and robust technique to probe electron flow within Complex I and gain valuable insights into the structural and functional organization of this respiratory complex *in situ*. Future developments toward clinical diagnosis of mitochondrial disorders or cancer can be envisioned.

3.4. Elaboration of a minimal model of DL generating states

The description of DL characteristics in terms of emitting-light states with lifetimes in the three above specified time intervals, along with the characteristic time course of the redox reactions that occur in Complex I [Verkhovskaya M. L. et al., 2008, Ransac S. et al., 2010] allowed us to propose a minimal model of DL-generating states produced during electron transfer (Fig. 18) consistent with the current DL data. In order to better follow up our reasoning and the model, in Fig. 17 we are reproducing Fig. 1 from [Baran I. et al., 2013, report 2013]. UV photoexcitation of FMN generates excited FMN singlet states that may either decay to the ground state by prompt fluorescence [Foster K.A. et al., 2006] or undergo intersystem crossing to long-lived triplet states which can further relax to metastable intermediate states [Swartz, T.E. et al., 2001].

In analogy with the Photosystem II case [Goltsev V. et al., 2005, Guo Y., J. Tan, 2009], the long lifetime of the triplet- or metastable-state species allows a series of photochemical reactions to occur in Complex I and produce secondary excitations, thus giving rise to the ultra-weak photon-induced delayed photoemission. The currently described S_1 states emitting blue or green/yellow light are most likely excited states of NADH or FMN_{ox}, respectively, that are produced after a series of forward and backward electron transfer steps reaching up to the Fe/S center N4 (Fig. 18A). A necessary condition for the two sequences shown in Fig. 18 Aa-b is that the primary oxidized NAD^+ molecule does not dissociate from Complex I during the entire time interval. Indeed, the average time for which NAD^+ remains attached to Complex I (~1 ms, [Verkhovskaya M.L. et al., 2008, Ransac S. et al., 2010]) is much larger than the overall lifetime of 29.3 μs estimated for the S_1 domain of the blue light emission traces (not shown). Next, the S_2 states emitting blue (or green/yellow) light may represent excited states of NADH (or FMN_{ox}) regenerated via backward charge recombination after the primary sequence of forward transfer steps reaching the center N2 (Fig. 18 Ba). The appearance of S_3 states probably involve charge transfer from center N1b to N5 and backwards, as well as from center N1a to N3 (Fig. 18C). In view of the similarities with the other spectral components, delayed emission of red light appears as well to be closely linked to Complex I.

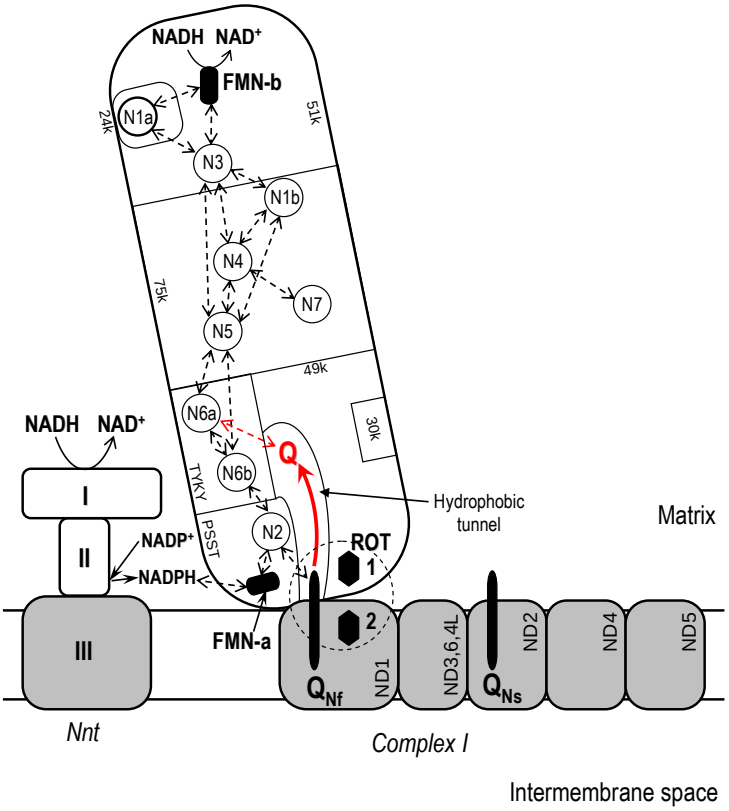

Fig. 17. Modular representation of Complex I architecture. The main seven hydrophilic and seven membranous subunits, labeled according to human Complex I subunit nomenclature, are schematically depicted. For simplicity, subunits ND3, ND6 and ND4L are comprised in a unique module. The relative positions of various subunits and Fe/S centers are only qualitatively pictured. Dashed arrows indicate possible electron transfer reactions. The two prosthetic FMN groups and their interaction with NADH/NADPH are illustrated. The two ROT (1 and 2) and two Q (Q_{Nf} and Q_{Ns}) sites are specified. The dashed circle encompasses the Q-binding pocket at the interface between the hydrophobic and the hydrophilic Complex I domains. Q may slide along the putative hydrophobic tunnel formed between the 49-kDa and PSST subunits, and interact with center N6a. The Nnt - Complex I interaction may regulate the reduction of FMN-a via the control of the local NADPH/$NADP^+$ ratio by Nnt [8] (here, only one Nnt monomer is illustrated; the three specific domains of the monomer, I, II (extramembrane domains) and III (membrane domain), are shown). [Baran I. et al., 2013, report 2013].

In consequence, we propose that red DL is most likely produced via dimol photoemission generated by two colliding molecules of singlet oxygen ($^1O_2$). Dimol luminescence can be observed at the characteristic wavelengths of 579, 634 and 703 nm [Khan A.U., M. Kasha, 1970, Boodaghians R. et al., 1982], with main emission at 634 nm. Thus, increased levels of superoxide produced by the semiflavone at the FMN-b (Fig. 18Ac-d, Fig. 18Bb, Fig. 18Ce) or FMN-a site (Fig. 18Bd,h), or by the ubisemiquinone at the Q site (Fig. 18Bc, Fig. 18Cd,f,g,i) could lead, particularly in the presence of superoxide dismutase, to the generation of significant levels of singlet oxygen [Khan A.U., 1978] and consequent dimol photoemission. We should note that our results differ from those of Mik et al. [Mik E.G. et al., 2006, 2008] who found that rotenone and other mitochondrial respiration inhibitors decrease the delayed (red) luminescence of endogenous proptoporphyrin IX (PpIX), which is synthesized inside the mitochondria. Rotenone inhibition of PpIX red DL appeared to be a process

mediated by increased levels of mitochondrial O_2 [Mik E.G. et al., 2006]. However, the experimental design used therein was based on the application of a PpIX precursor (5-aminolevulinic acid hydrochloride, ALA) to enhance the intracellular PpIX concentration. In the absence of ALA, red DL of HeLa cells was virtually undetectable (Fig. 4a in [Mik E.G. et al., 2006]). Under our conditions (excitation at 337 nm, vs. 405 nm in [Mik E.G. et al., 2006] or 510 nm in [Mik E.G. et al., 2008]), we observed a strong enhancement of red DL by rotenone, which could suggest that, at least in Jurkat cells, singlet oxygen is the likely dominant generator of red DL observed upon excitation at 337 nm. On this basis, our current DL data suggest that the average time elapsed since the generation of semiflavone at FMN-b until the collision of the emerging $^1O_2$ with a second singlet oxygen situated in close vicinity is 13.3 μs (Fig. 18Ac). For simplicity, we also assume that the other two sites of superoxide generation in Complex I, namely FMN-a and Q, exhibit the same kinetics of dimol photoemission, with an overall time of electron transfer from semiflavone/semiquinone to molecular oxygen, dimol production and radiative decay, of 13.3 μs. Moreover, our DL data are best explained by assuming that center N2 is reduced by NADH within 90 μs, in accord with previous reports [Verkhovskaya M.L. et al., 2008], which provides a characteristic time of 54 μs required for the electron transfer from center N6b to N2 (Fig. 18Ba).

It is worth nothing that the two values derived above explain very well the dominant kinetic component of both blue and green/yellow (140 μs derived from DL emission curves, not shown), as well as red light emission from S_2 states (148 μs) produced via NADH reduction of N2, followed by reverse electron transfer to FMN-b and NADH (Fig. 18Ba,b). However, we propose that the prominent S_2 component (129 μs) of red DL is produced via reduction of ubiquinone by the first electron of NADH received from center N2 (estimated time, 20 μs), generation of superoxide and then singlet oxygen dimol by the usual pathway (Fig. 18Bc). In the presence of ROT, the ubisemiquinone becomes unstable, dissociates from the Q_{Nf}-site and reduces O_2 to superoxide [Ohnishi S.T. et al., 2005]. In the absence of rotenone, ubisemiquinone remains attached to the Q_{Nf}-site (for which it has a high affinity) and is further reduced to ubiquinol ($Q_{Nf}H_2$) by the second incoming electron from N2. $Q_{Nf}H_2$, which cannot react with molecular oxygen because the reaction is spin forbidden [Albracht S.P.J. et al., 2011], participate in electron transfer within the membrane domain and in proton translocation. In consequence, ROT will increase the red light emission from the semiquinone radical produced at the Q-site via reduction by NADH. The slower component (390 μs) of red DL may be produced in a similar manner, via reduction of flavin FMN-a by NADH through center N2, and subsequent interaction with O_2 (Fig. 18Bd). We estimated that in the presence of rotenone, the mean time for electron transfer from reduced center N2 to FMN-a is 284 μs in situ, which suggests that the likelihood for N2 to reduce ubiquinone is 14 times higher than to reduce FMN-a. On the millisecond timescale, delayed red light emission may involve electron transfer between centers N1b and N5, or transfer from center N1a to N3, and subsequent superoxide production at the FMN-b, FMN-a or Q sites (Fig. 18Cd-e,g-i). In addition, we propose that the distinct red-DL component with decay time of 3.87 ms is associated with the reduction of ubiquinone by center N6a. Nevertheless, the long time required for this charge transfer reaction is compatible with a reduced likelihood of a process in which the long, flexible tail of ubiquinone manages to arrange itself inside the putative hydrophobic tunnel formed between the 49-kDa and PSST subunits of Complex I [Albracht S.P.J. et al., 2011] (Fig. 17).

A. S_1

a) 32 μs (Blue, Green/Yellow)

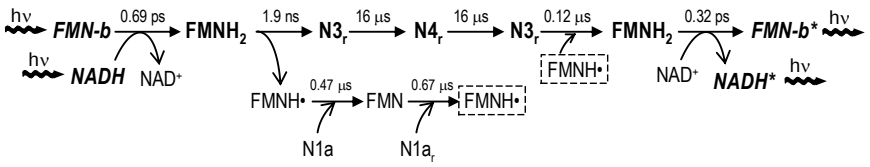

b) 37 μs (Blue, Green/Yellow)

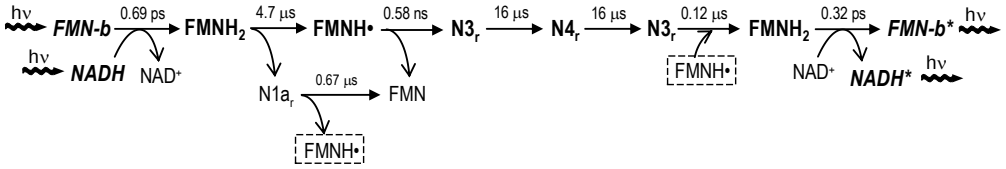

c) 13.3 μs (Red)

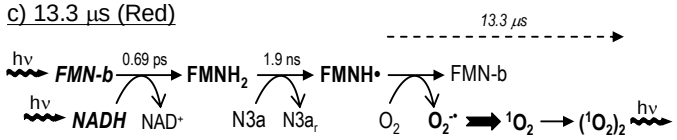

d) 18 μs (Red)

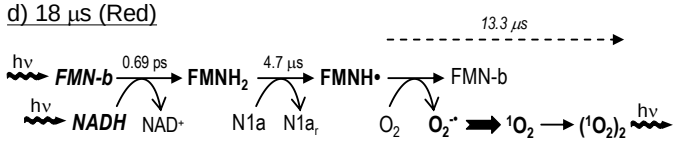

B. S_2

a) 135 μs/140 μs (Blue, Green/Yellow)

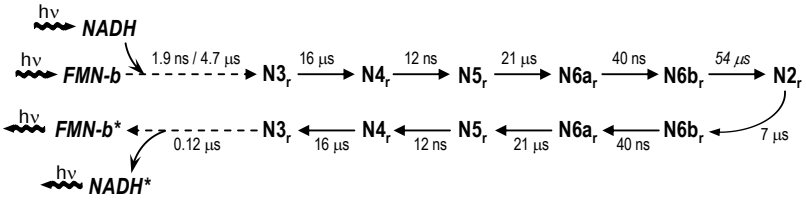

c) 124 μs/129 μs (Red)

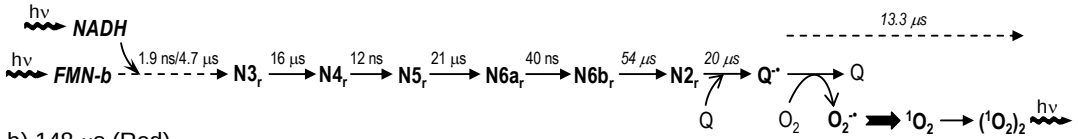

b) 148 μs (Red)

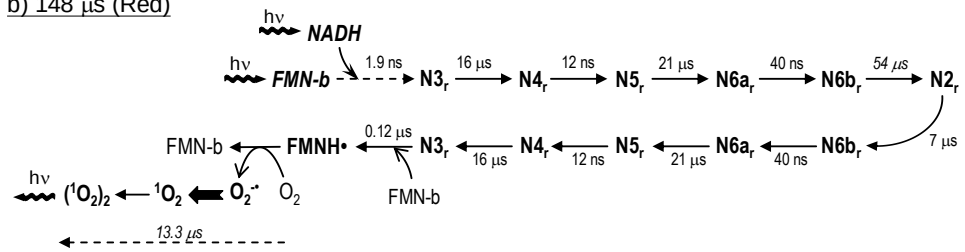

d) ≈390 μs (Red)

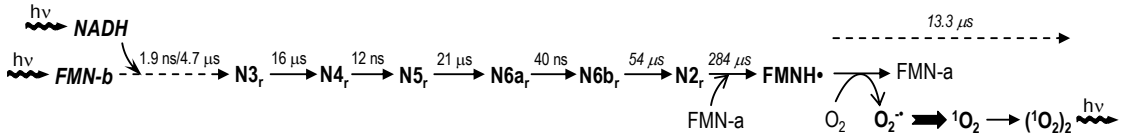

C. S_3

Fig. 18. Minimal model of DL-generating states produced during electron transfer in Complex I, in accordance with data presented in Figs. 4-9. S_1, S_2 and S_3 classes of states are discussed separately in panels **A**, **B** and **C**, respectively. Arrows indicate the main product(s) resulting after electron transfer in the respective step. The reduced form of Fe/S centers is indicated by the subscript "r". Individual time constants of electron transfer steps are taken from [Ransac S. et al., 2010], except the values estimated in this work (*italicized*). Regenerated $FMNH^{\bullet}$ which can participate in subsequent reactions is indicated by a dashed rectangle. Dashed arrows at the beginning of the reaction series in **B** and **C** indicate the two possible electron transfer modalities shown in **A**b and **A**c. Dashed arrows at the end of the reaction series indicate the time elapsed between the collision of the O_2 molecule with the $FMNH^{\bullet}$ or $Q^{\bullet}$ radical, and the ensuing dimol photoemission.

Although the crystal structure of Complex I isolated from two prokaryotic systems (*E. coli, T. thermophilus*) does not present clear evidence for this scenario [Berrisford J.M., L.A. Sazanov, 2009], it is possible that it does not accurately reflect the constitution of mammalian Complex I [Blinova K. et al., 2008], which could present distinct particularities, especially in its native mitochondrial environment. Accordingly, our data suggest that both situations are possible, however the protrusion of ubiquinone into the hydrophobic tunnel up to cluster N6a appears to be a rather rare event, which could essentially be facilitated by the binding of rotenone at site 1.

3.5. Evaluation of apoptosis and EGCG dose-dependent clonogenic survival

We have evaluated the cytotoxicity of EGCG, applied alone or in combination with menadione, in human leukemia Jurkat T cells, and investigated some of the underlying mechanisms related to induction of apoptosis. In order to investigate the clonogenic survival we have proceeded as described in the following. After treatments, as previously described, cells were washed thoroughly with warm PBS and plated in 96 well plates at a plating density of 4 or 6 cells/well in 100 μl of complete medium per well. After 3-4 weeks of incubation, plates were inspected by microscopy and wells containing at least one colony with >50 cells were scored equally as positive wells and counted. The plating efficiency was calculated by the ratio of the theoretical Poisson density of the number of negative wells observed, against the initial plating density, i.e. ln[96/(no. of negative wells)]/(plating density) × 100 (Chen et al., 2001). Clonogenic survival was calculated as the ratio between the plating efficiency of treated and control cells, respectively. *Data fitting* was performed using the software Origin, version 7.5. Unless otherwise stated, monophasic inhibitory and stimulating effects of various agents on a measured quantity (y) were fitted to the functions:

$$y = y_0 + (y_{max} - y_0)\,[1 - x^h/(IC_{50}{}^h + x^h)] \quad (1)$$

and

$$y = y_0 + (y_{max} - y_0)\,x^h/(EC_{50}{}^h + x^h) \quad (2)$$

respectively, where x and h denote concentration and Hill coefficient, respectively, y_0 and y_{max} are the minimal and maximal values of y, respectively, and IC_{50} and EC_{50} are the corresponding half maximal inhibitory and the half maximal effective concentration of the agent, respectively.

Antiproliferative effects of EGCG, MD and their combination. Acute treatments with EGCG applied for 1 h induced a dose-dependent decrease in the clonogenic survival of Jurkat cells (Fig. 19A). The EGCG concentration required for reducing clonogenicity to 50% was 117 μM (Table 2), and the associated Hill coefficient (3.17) indicated a high degree of cooperativity between the EGCG-specific mechanisms underlying the cell death process.The combination EGCG:MD demonstrated a significant synergic character. Thus, the dose-dependent cytotoxic effect of menadione applied alone for 20 min. was characterized by an IC_{50} of 66.8 μM and a Hill coefficient of 1.37 (Fig. 19B, Table 3), suggesting cooperative interaction between the MD-specific processes that mediate the observed growth-suppressive effect.

Table. 2. EGCG specific parameters (IC_{50} or EC_{50}, median effect dose; *h*, Hill coefficient) associated with clonogenic survival in Jurkat cells after acute exposure to EGCG.

Parameter	Clonogenic survival
IC_{50}/EC_{50} (μM)	117
h	3.17

Preincubation with 50 μM or 100 μM EGCG for 1 h reduced the median effect dose of menadione to 32.7 μM and 9.48 μM, respectively, without affecting significantly the Hill coefficient (Table 3). At a lower concentration (5 μM), EGCG did not interfere in any measurable way with the cytotoxic effect of menadione (not shown). The combination indexes of the two EGCG:MD combinations yielding a clonogenic survival of 10% were relatively similar (0.69 and 0.51 for 50 μM and 100 μM M EGCG, respectively) and indicated synergic interaction between the two agents. For an effect level of 1% clonogenic survival, the corresponding combination indexes were even lower (0.61 and 0.27, respectively).

The Annexin V/PI apoptosis assay revealed that MD at concentrations up to 100 μM, either applied alone or in combination with 50 μM or 100 μM EGCG for 1 h, decreased significantly cellular viability within 24 h from exposure, in a dose dependent manner (Fig. 19C, D). In contrast, EGCG (50 μM or 100 μM EGCG) applied for 1 h did not have major effects on cellular viability, whereas the EGCG:MD combination displayed noticeable synergic features of cytotoxicity associated with considerable apoptosis (Fig. 19C, D).

Table 3. Menadione-specific cytotoxicity parameters derived from clonogenic survival after acute exposure to MD, in the absence or presence of EGCG at indicated concentrations.

Parameter	[EGCG], μM		
	0	50	100
IC_{50} (μM)	66.8	32.7	9.48
h	1.37	1.33	1.59

Experiments conducted with EGCG and/or MD treatments at physiologically relevant parameters showed that levels compatible with feasible clinical administration schemes can exert potent antiproliferative effects on Jurkat cells. Thus, exposure for 24 h or 48 h to 10 μM EGCG combined with 10 μM MD elicited efficient death rates, which could be observed right after the treatment (Fig. 20A-C).

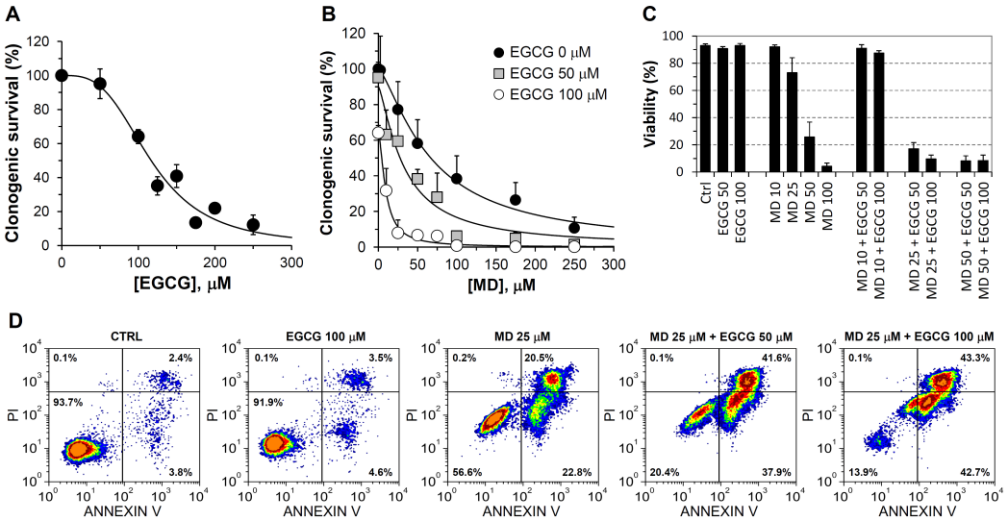

Fig. 19. Cytotoxicity of EGCG and MD after acute treatments is associated with a dose-dependent decrease in clonogenic survival of Jurkat cells and apoptosis induction. Cells were exposed to EGCG for 1 h (**A**), or to MD for 20 min., following 1-h preincubation with EGCG at indicated concentrations (**B**). Curves were generated by data fitting to Eq. 1. (**C**) Cellular viability following 1-h exposure to EGCG and/or MD at indicated concentrations (in μM). Flow cytometric determinations were done by the Annexin V/PI assay after 24 h from drug removal. Viability is expressed as the fraction of Annexin V- and PI-negative cells. (D) Representative bivariate plots showing apoptosis induction in Jurkat cells exposed to EGCG, MD or combinations at indicated doses. Cell fractions in each quadrant are indicated as % of gated events.

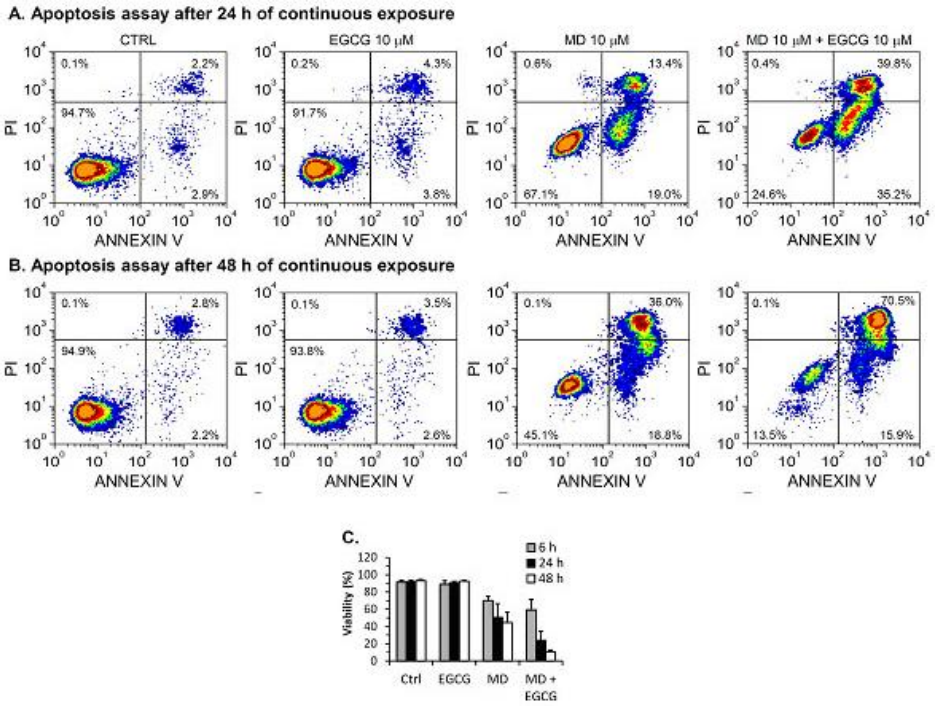

Fig. 20. Induction of apoptosis and oxidative stress in Jurkat cells exposed to 10 μM MD and/or 10 μM EGCG. Typical Annexin V/PI bivariate plots obtained by flow cytometry after 24 h (**A**) or 48 h (**B**) of continuous exposure. Cell fractions in each quadrant are indicated as % of gated events. (**C**) Cellular viability was determined as the fraction of Annexin V- and PI-negative cells 24 h after 6-h exposure with the medium changed every 2 h, or immediately after continuous exposure for 24 h or 48 h, as indicated.

In particular, this combination was highly effective in cell killing, producing a viable cell fraction as low as 10.8 ± 1.8% after 48 h of exposure, whereas EGCG alone (10 μM) had no measurable impact on cellular viability, and MD alone (10 μM) decreased viability to 44.6 ± 12.4%, suggesting a synergic interaction between the two agents. The Annexin V/PI assay used to obtain these values also indicated that MD and, more prominently, the EGCG:MD combination triggered extensive apoptosis within 24 h and 48 h of exposure (Fig. 20A,B).

In conclusion, this study provides some novel insights into the cytotoxic effect of EGCG on human leukemia Jurkat T cells. First, short-term (1 h) treatments indicated a dose-dependent decrease in cellular viability, which was characterized by a highly cooperative interaction, likely involving three EGCG molecules. The cell killing ability of EGCG was synergistically enhanced by menadione. Based on a clonogenic survival assay, relevant values of the combination index (0.3 - 0.6) were obtained. Moreover, flow cytometric determinations on cells double stained with Annexin V and PI suggested that the cytotoxic effect of EGCG applied alone or in combination with MD is accompanied by apoptosis induction.

4. Discussion

On the basis of our main results, obtained from the studies carried out in the frame of the present project, by using the delayed luminescence method, we can make the followings statements: 1) DL is closely related to the level of oxidized FMN, which is found primarily in the mitochondria [Gaspers L.D., A.P. Thomas, 2008, Heikal A.A., 2010], 2) DL is also linked to the level of NADH, the substrate of mitochondrial Complex I, 3) ROT, a specific inhibitor of Complex I, affected DL considerably, and 4) MD and QC, which interact robustly with Complex I, also affected DL significantly, all our results reinforce the idea that mitochondrial Complex I plays a major role in the ultra-weak photon-induced delayed photoemission in Jurkat cells. On the basis of all our results obtained in the frame of the present project, we can make a number of observations concerning the correlation between the mitochondrial metabolism and delayed luminescence.

Perhaps the most physiologically relevant outcomes of our investigations derive from the finding that the DL yield depends in a Hill-like fashion on the level of NADH as well as that of oxidized flavine mononucleotide (FMN_{ox}), with apparent Hill coefficients of 4.3. Moreover, spectral DL analysis indicated different degrees of cooperativity of both NADH and FMN_{ox}, reflected in differing Hill coefficients associated with blue, green/yellow and red light emission, namely 3.9, 7.2 and 2.8, respectively. In addition, fluorimetric measurements of NADH and FMN_{ox} levels indicated that rotenone binding exhibits an apparent Hill coefficient of 2.0-2.4, suggesting that Complex I functions mainly as a dimer in intact Jurkat cells. Based on these findings, we propose that blue and red DL is produced predominantly by dimeric Complex I, whereas green/yellow DL arises mainly from tetrameric Complex I. At first sight, these results could suggest a cooperative action of the NADH and NADPH sites of a Complex I monomer, as well as cooperativity between both oxidized flavins (i.e., FMN-a and FMN-b [Albracht S.P.J. et al., 2011]), to generate DL-specific states, corroborated by the cooperative interaction between all monomers that are coupled within a Complex I oligomeric form. Such a cooperativity between sites situated at the two extremities of the hydrophilic sector of Complex I has to

involve a long-range interaction (which nevertheless has been documented [[Hano N. et al., 2003, Sazanov L. A., 2007, Berrisford J.M., L.A. Sazanov, 2009]]) and might reflect that in the particular Complex I conformation induced by specific modulators like rotenone, menadione and quercetin, the affinity of NADPH for its site is increased in the NADH-bound Complex I. However, having in view that the concentration of NADPH in the matrix is generally much lower than that of NADH (reviewed in [Mayevsky A., G.G. Rogatsky, 2007]), a more plausible interpretation can be drawn from the idea of a tight interplay between Complex I and Nnt (nicotinamide nucleotide transhydrogenase), a mitochondrial enzyme catalyzing the reaction NADH + $NADP^+ \leftrightarrow$ NADPH + NAD^+. It is suggested [Albracht S.P.J. et al., 2011] that Nnt (a homodimer) can form a heteromer with Complex I and thus regulate the NADPH/$NADP^+$ ratio in the vicinity of the NADPH site of Complex I (Fig. 17). By this mechanism for example, Nnt co-operates with Complex I in the attenuation of hydrogen peroxide generation by Complex I [Albracht S.P.J. et al., 2011]. It is thus conceivable that *in situ*, NADH binding to its site in Complex I leads somehow to the stabilization of the Complex I - Nnt heteromer, hence increasing the apparent rate (and affinity) of NADPH binding to its distal site on Complex I. Thus, we propose that, in order for ROT-, MD- or QC-bound Complex I to generate DL, one NADH molecule must be bound to its site on Complex I, one NADH molecule must associate with the Nnt monomer that is docked on the comer of Complex I, and Complex I and Nnt must form a tightly bound heteromer. Finally, in the same particular conformation of Complex I, binding of NADH and similarly, NADPH, to their corresponding sites enhance the rate of FMN-b and FMN-a oxidation, respectively. Therefore, an apparent Hill coefficient of 2 obtained for NADH per Complex I monomer will be closely linked to an apparent Hill coefficient of 2 characteristic for oxidized FMN. In the Nnt-Complex I heterotetramer, the NADH binding sites situated on the two monomers of Complex I, as well as the two NADH sites on the two Nnt monomers, must interact cooperatively. Thus, our results are consistent with the notion that in Jurkat cells the main structural organization of mitochondrial Complex I is most likely a supercomplex comprised of one Complex I dimer and one Nnt dimer. In favor of this, the concentrations of Complex I and Nnt in bovine-heart submitochondrial particles have been found to be closely similar [Albracht S.P.J. et al., 2011].

At this point, it should be recalled that multiple dinucleotide (NAD(H) and NADP(H)) binding sites were identified within the sequence of Complex I, and, consistent with this, five subunits isolated from Complex I were found to bind NADH and/or NADPH [Yamaguchi M. et al., 2000]. Steady-state kinetic studies of the transhydrogenase activity of Complex I also indicated that a single dinucleotide-binding site is incompatible with the data [Zakharova N.V. et al., 1999]. Moreover, cooperative binding of NADH in Complex I, with an associated Hill coefficient of 2.3 [Suzuki H., T.E. King, 1983] or 2.6 [Dooijewaard G., E.C. Slater, 1976], has been reported by different groups. In addition, in Complex I preparations where the Hill coefficient for NADH binding was 2.3, the corresponding Hill coefficient for rotenone binding was found to be 1.1 [Suzuki H., T.E. King, 1983]. We remark that the ratio no. of NADH molecules/no. of ROT molecules bound to Complex I derived in our study (≈2) is in good accord with these figures, but, based on the number of NADH and FMN molecules involved (two of each per bound molecule of rotenone), suggests that the second active dinucleotide site must interact with the second flavin (i.e., FMN-a). However, at the moment the only well defined NADH-binding site of Complex I remains that situated in the FMN-b containing, 51 kDa subunit of the complex [Yamaguchi M. et al., 2000, Sazanov L.A., 2007, Berrisford J.M., L.A. Sazanov,

2009]. Therefore, in the absence of conclusive knowledge of a functional NADH site which would be able to interact with FMN-a, we believe that the hypothesis of heteromeric Nnt-Complex I coupling can reasonably explain our DL data. Moreover, the presumed ability of Complex I to form oligomers in the native inner membrane of intact cell mitochondria is in line with recent evidences of the existence of large functional respirasome supercomplexes in various combinations of monomers, dimers or trimers of individual respiratory complexes, with different stoichiometries [Stroh A. et al., 2004, Marques I. et al., 2007]. So, it is conceivable that *in situ*, Complex I can form dimers, as also suggested by a number of previous studies [Brink J. et al., 1988, R. van Belzen R., et al., 1990, Stroh A. et al., 2004, Krause F. et al., 2004, Marques I. et al., 2007], or even tetramers [Boekema E.J.et al., 1982]. To date, dimeric Complex I has been detected in fungal mitochondria, and it has been proposed that such dimers may occur in organisms possessing alternative respiratory enzymes [Krause F. et al., 2004, Marques I. et al., 2007]. It is thus possible that under the ROT blockage the alternative oxidase is activated in Jurkat cells, hence increasing the likelihood of Complex I aggregation. In favor of our hypothesis on the formation of Complex I dimers or higher oligomers, we found in a different set of experiments that quercetin induces in Jurkat cells, long after drug removal, a persistent mitochondrial hyperpolarized state, which is inhibited by rotenone in a biphasic manner, with corresponding Hill coefficients of 1.2-1.4 and 2.8-3.6, respectively [Baran I. et al., 2014]. Moreover, those measurements involved the fluorimetric detection of the fluorescent emission of a well established fluorescent indicator, JC-1, not that of NADH or FMN. Hence, these latter results lend further support for the concept of cooperative interaction between 2 and 3-4 rotenone binding sites, respectively. In addition, an independent non-fluorimetric assay conducted here on the basis of clonogenic survival determinations (report 2013, Fig. 2A) also indicated cooperativity between at least two ROT binding sites This excludes the idea that the current outcomes might reflect some potential fluorescence artifacts rather than the actual dependence of NADH and FMN levels on the ROT dose. In conclusion, the human leukemia Jurkat cell line appears to be an appealing candidate for further studies investigating the possible formation of Complex I oligomers in mammalian cells. Thus, on the basis of our current results we may suggest that in Jurkat cells Complex I oligomers are formed, at least in the presence of ROT, QC or MD, and may exist in either dimeric or tetrameric form, with an abundance ratio of 3:2. Approximately 50-90% of Complex I is currently thought to be associated with dimeric Complex III in supercomplexes that may also contain 1-4 subunits of Complex IV [Krause F. et al. 2004]. Interaction between Complex I and complex III within the respirasomes was found to be essential to the activity and stability of Complex I [Eichler M. et al., 2005]. Importantly, the existence of even larger supercomplexes containing multiple monomers of Complexes I, III and IV was unambiguously confirmed [Krause F. et al., 2004]. It is therefore possible that our assay detected mixed responses originating from such supercomplexes assembled from oligomeric Complex I and oligomeric Complex III, having in view the peculiar effects of rotenone and/or antimycin A on flavin autofluorescence observed in our experiments. Knowledge of monomeric/oligomeric Complex I specific distribution may be significant for the understanding of the molecular and functional properties of the respiratory complexes and supercomplexes in physiological or pathological conditions.

Our fluorimetric measurements [Baran et al., 2013, 2014, report 2013] also demonstrated, contrary to expectations [Gaspers L.D., A.P. Thomas, 2008], a strong linear correlation between the mitochondrial level of NADH and that of oxidized

FMN in Jurkat cells treated with Complex I targeting agents like ROT, MD and QC. This rather unusual feature was observed previously in muscle tissue [Kuznetsov A.V. et al., 1998] and human monocytes [Kindzelskii A., H.R. Petty, 2004], where rotenone was reported to increase flavoprotein emission. The correlation established here could suggest that in Jurkat cells the ROT-, MD- or QC-bound Complex I accelerates the electron transfer from reduced FMN, either towards the neighbor Fe/S centers or backwards, to the NAD^+ molecule, if the latter has not dissociated yet from FMN. In any case, assuming that the total level of mitochondrial flavins does not change significantly during the treatment, the observed increase in the fluorescence of FMN_{ox} at increasing levels of NADH definitely reflects an overall increase in the population (and relative dwell time) of the oxidized state of FMN and a corresponding decrease in the population (and relative dwell time) of the semi- or fully reduced states of FMN. Having in view that a NADH increase does not induce by itself an increase in the level of FMN_{ox}, as demonstrated by experiments employing the Complex III inhibitor, Antimycin A, we infer that ROT, MD and QC most likely induce a conformational change in Complex I, in which the density of the FMN_{ox} population is directly related to the level of NADH in the matrix, hence with the apparent residence time of $NADH/NAD^+$ at its binding site in Complex I (since binding of NADH to the enzyme results in a long-range conformational change at the membrane interface (quinone-binding pocket) [Hano N. et al., 2003, Sazanov L.A., 2007, Berrisford J.M., L.A. Sazanov, 2009], it is conceivable that the reverse situation is also possible). A likely explanation may be that the binding of rotenone or menadione/quercetin to Complex I *in situ* inhibits or stimulates, respectively, the dissociation of NAD^+ from Complex I following reduction of FMN by NADH, and that associated NAD^+ favors the oxidized state of FMN in this particular conformation. However, since rotenone does not affect the reduction kinetics of neither of the Fe/S clusters [Albracht S.P.J. et al., 2011], it seems more likely that the semiflavine radical $FMNH^\bullet$ which is produced rapidly after reduction of center N3a by $FMNH_2$, dislocates within the FMN binding cavity and produces a conformational change of the protein which would allow the access to molecular oxygen (even in the presence of NAD^+ in the substrate binding cleft), leading to subsequent production of superoxide. Regenerated FMN_{ox} can then rebind with high affinity to its site. Moreover, high levels of NADH appear to stimulate the dissociation of $FMNH^\bullet$ from the FMN site [Vinogradov A.D, 2008], which lends further support for our interpretation. Thus, our data suggest that rotenone increases, whereas menadione and quercetin decrease the probability of O_2 reduction by $FMNH^\bullet$, via modulation of the NADH level but also by conformational facilitation of the NADH effect on $FMNH^\bullet$. In addition, since both quercetin and menadione decrease $[NADH]_m$ and $[FMN_{ox}]$ and also have closely similar effects on DL [Baran I. et al., 2010, the studies in the frame of the present project] it is expected that both agents share a common binding site and operate by similar mechanisms at the level of Complex I in Jurkat cells. Reports that quercetin can act as a coenzyme Q-mimetic molecule [Sandoval-Acuña C. et al., 2012] or decrease the ROS production by Complex I [Lagoa R. et al., 2011] further substantiate the current proposal that menadione and quercetin decrease the affinity of NAD^+ for the reduced form of Complex I (the apparent $K_d \approx 10$ μM under normal conditions [Vinogradov A.D., 2008]) by stimulating the dissociation of NAD^+ from reduced Complex I. In turn, the vacancy in the NADH site hampers the detachment of $FMNH^\bullet$, and so the inability of the flavin radical to access dioxygen leads to decreased superoxide production. The observation that rotenone exerts opposed effects in H_2O_2 production by mitochondria, although its site is situated in the same

hydrophobic cavity at the matrix/membrane interface [Lagoa R. et al., 2011], is also in agreement with our results. Quercetin and menadione are likely to inhibit the accessibility of ubiquinone to both Fe/S centers N2 and N6a, as well as the reduction of N2 by FMN-a, hence explaining the considerable decrease of DL observed especially on the S_2 and S_3 timescales [Baran I. et al., 2010]. Interestingly, in the rat brain and heart mitochondrial preparations of Lagoa and collaborators, quercetin exercised its inhibitory effects on Complex I without affecting the respiration (oxygen consumption) rate [Lagoa R. et al., 2011], suggesting that quercetin is able to receive both electrons from N2 and redirect them to Q_{Ns} without the destabilization of the intermediary radical, thereby acting as a substitute for ubiquinone [Lagoa R. et al., 2011]. However, since menadione produces superoxide at Complex I by forming a semiquinone [Xu X., E.A. Arriaga, 2009, Floreani M., F. Carpenedo, 1992], presumably after accepting one electron from center N2, we infer that the main mechanism responsible for the observed effects of menadione and quercetin on DL are caused by the inhibition of: 1) semiflavine lifetime (indirectly, via a NADH/NAD^+ mediated effect), 2) ubiquinone reduction at center N6a, and 3) N2 reduction by FMN-a, whereas rotenone enhance DL by stimulating all these processes but also the backward electron transfer from center N2 to FMN-b (due to an increased pool of electrons dwelling inside Complex I). In addition, having in view that the rate-limiting step that defines the enzymatic activity of Complex I is the dissociation of NAD^+ from its site, which has a typical lifetime ~1 ms under normal conditions [Verkhovskaya M.L. et al., 2008, Ransac S. et al., 2010], our results support the idea that ROT inhibits, whereas MD and QC stimulate Complex I activity by inhibiting or stimulating the dissociation of NAD^+.

Our current DL data indicate that the apparent constant of NADH or FMN_{ox} dissociation from ROT-, MD- or QC-associated Complex I in Jurkat cells is 2.92 or 2.65 times higher, respectively, than the resting concentration of total (free + bound) NADH or FMN_{ox} (denoted here as $[NADH]_0$ and $[FMN_{ox}]_0$, respectively). On the other hand, from spectrofluorimetric data we could estimate that NADH exerts its local effect on the neighbor FMN at the level of monomeric Complex I with an apparent $K_d = 8.25 \times [NADH]_0$ (derived by fitting the data in Fig. 3C from [Baran I. et al., 2013] to a single NADH -binding site model, with estimated Hill coefficient 1.2,). The affinity of NADH for monomeric Complex I generally varies from about 20-50 μM in the reduced form of the enzyme to 100 μM in the oxidized enzyme. A crude calculation based on an intermediate value of 60 μM provides an estimate of the content of NADH in the mitochondrial compartment of Jurkat cells of about 60 μM/8.25 = 7.3 μM. We notice that this figure is highly consistent with estimates from different cancer cell lines: ~7 μM and ~6 μM (derived from data presented in Fig. 6 and Table 4 in [Villette S. et al., 2006]) in two malignant human esophageal epithelial cell lines, OE33 and OE21, respectively. Moreover, the apparent K_d of NADH binding to oligomeric Complex I in Jurkat cells appears to be significantly lower (2.92 × 7.3 μM ≈21 μM) than in the monomeric enzyme (60 μM), substantiating the notion of cooperative interaction between the monomers. In addition, the abovementioned fit to the data presented in Fig. 3C from [Baran I. et al., 2013] supplied also a maximal relative level of FMN equal to $11.63 \times [FMN_{ox}]_0$. The cellular content of total (free + bound, oxidized + reduced) FMN is considered to be ~5-50 μM [Eichler M. et al., 2005] (these figures are based on a wide set of data in [Pérez-Ruiz T. et al., 2001] and can be derived assuming a cellular protein density $\rho = 1.05 \times 10^{-12}$ g/fl [Skog S. et al., 1987, Vinnakota K.C., J.B. Bassingthwaighte, 2004]). The rotenone sensitivity of

Complex I in our experiments (K_d = 33 μM) suggests that the concentration of FMN in Jurkat cells is roughly 50 μM, based on the fact that rotenone inhibits Complex I activity at concentrations approaching the FMN content of the enzyme [Hatefi Y., J.S. Rieske, 1967]. This also validates our current assumption that the FMN fluorescence signal we recorded in Jurkat cell suspensions originates mainly from Complex I-associated FMN. So, assuming that the maximal relative level of FMN is 11.63 × $[FMN_{ox}]_0$ = 50 μM, we obtain $[FMN_{ox}]_0$ = 4.3 μM and $[FMN_{red}]_0$ = 45.7 μM, where FMN_{red} stands for (semi- + fully-) reduced FMN. In addition, the apparent affinity of FMN for oligomeric Complex I in Jurkat cells appears to be, in a raw approximation, 2.65 × 4.3 μM = 11.4 μM. It is widely accepted that FMN binds tightly but non-covalently to the first active FMN site (FMN-b) of the apoenzyme; however, we could not find in the literature but one single quantitative report of the corresponding dissociation constant, which was determined to be 0.4 and 10.0 nM in bovine heart submitochondrial particles at pH 9.0 and 10.0, respectively [Gostimskaya I.S. et al., 2007]. It was concluded therein that FMN reduction weakens the binding of FMN to Complex I [Gostimskaya I.S. et al., 2007]. The second FMN site (FMN-a) has not been characterized yet. However, the K_d estimated here (11.4 μM) is similar to the K_d = 4 μM reported for FMN binding to the clostridial NADH oxidoreductase [Barnes S., J.G. Spenney, 1980] or the K_d = 5 μM reported for FMN binding to the NADPH:FMN oxidoreductase of Vibrio harveyi [Liu M. et al., 1997]. Our result also resembles the case of particular flavodoxins or flavodoxin-like proteins that exhibit an unusually weak FMN binding (K_d = 1-2 μM, compared with typical values of ~1-10 nM [Ji H.F. et al., 2006, Bui S.H. et al., 2012]). Nevertheless, it is clear that the aforementioned values indicate a low FMN affinity for ROT-, MD- or QC-bound Complex I in Jurkat cells, which may suggest that the specific conformation of the ROT-, MD- or QC-bound protein decreases considerably the intrinsic affinity of FMN for Complex I. This feature could reflect either a constitutive mutation in the FMN binding site [Bui S.H. et al., 2012] or an altered H-bond network in the FMN environment [Nogués I. et al., 2004] in the modified conformation of the enzyme, which could hinder the access of the 5'-phosphate group of FMN to the phosphate-binding subsite of the FMN-binding site [Murray T.A., R.P. Swenson, 2003]. Indeed, it has been asserted that a reduced number of hydrogen bonds between the apoprotein and the phosphate group of FMN are a major cause for weak FMN binding [Ji H.F. et al., 2006]. Whatever the case, our data seem to support the notion that the binding of ROT, MD or QC to Complex I does not affect dramatically the overall affinity of NADH for the protein, whereas it greatly reduces the apparent affinity of FMN.

5. **Conclusion**

We present evidence that the ultra-weak photon-induced delayed photoemission of intact Jurkat cells originates mainly from mitochondrial Complex I, which appears to function predominantly as a dimer (with a relative frequency of about 60%) and less frequently as a tetramer (with a relative frequency of about 40%) in this cell type. Complex I oligomers appear to exhibit cooperative interaction between monomers at the level of the rotenone site 1, NADH/NADPH sites and FMN-b/FMN-a sites. Moreover, in individual monomers, both pairs of pyridine nucleotide (NADH/NADPH) binding sites and flavin (FMN-b/FMN-a) binding sites, which are situated at the two extremities of the extramembranous domain of Complex I, display strong cooperativity in the binding of their specific ligands. In addition, the

timescales of various electron transfer steps involving the formation of flavin and ubisemiquinone radicals with subsequent production of superoxide can be estimated from delayed red-light emission. All these findings raise the attractive possibility that DL spectroscopy could be used as a reliable, sensitive and robust technique to probe electron flow within Complex I and gain valuable insights into the structural and functional organization of this respiratory complex in situ. Future developments toward clinical diagnosis of mitochondrial disorders or cancer can be envisioned.

6. References

Albracht, S.P.J., A.J. Meijer, J. Rydström, J. Bioenerg. Biomembr. 43 (2011) 541-564.

Baran, I., C. Ganea, A.Scordino, F.Musumeci, V.Barresi, S.Tudisco, S.Privitera, R.Grasso, D.F.Condorelli, V.Baran, E.Katona, M-M.Mocanu, M.Gulino, R.Ungureanu, M.Surcel, C.Ursaciuc, Cell Biochemistry and Biophysics 58 (2010) 169-179

Baran, I., C. Ganea, S. Privitera, A. Scordino, V. Barresi, F. Musumeci, M. M. Mocanu, D. F. Condorelli, I. Ursu, R. Grasso, M. Gulino, A. Garaiman, N. Musso, G. A., P. Cirrone, G. Cuttone., Oxidative Medicine and Cellular Longevity 2012 (2012) Article ID 498914 (14 pp)

Baran, I., D. Ionescu, S. Privitera, A. Scordino, M. M. Mocanu, F. Musumeci, R. Grasso, M. Gulino, A. Iftime, I. T. Tofolean, A. Garaiman, A. Goicea, R. Irimia, A. Dimancea, C. Ganea, Journal of Biomedical Optics 18 (2013) 127006

Baran, I., D. Ionescu, A. Filippi, M. M. Mocanu, A. Iftime, R. Babes, I. T. Tofolean, R. Irimia, A. Goicea, V. Popescu, A. Dimancea, A. Neagu, C. Ganea, (2014) Leukemia Research**,** 38, 7 pp. 836-849

Baran I, Ganea C. et al. 2009. *Rom J Phys* 54: 557-569]

Barbouti, A. et al. 2007. *Free Radic Biol Med* 43: 1377-1387

Barnes, S., J.G. Spenney, Clin. Chim. Acta 107 (1980) 149-154.

van Belzen, R., M.C.M. van Gaalen, P.A. Cuypers, S.P.J. Albracht, Biochim. Biophys. Acta 1017 (1990) 152-159.

Berrisford, J.M., L.A. Sazanov, J. Biol. Chem. 284 (2009) 29773-29783.

Brink, J., E.J. Boekema, E.F.J. Van Bruggen, Electron Microsc. Rev. 1 (1988) 175-199.

Boekema, E.J., J.F.L. Van Breenen, WKeegstra, E.F.J. Van Bruggen, S.P.J. Albracht, Biochim. Biophys. Acta 679 (1982) 7-11.

Boodaghians, R., P.M. Borrell, P. Borrell, K.R. Grant, J. Chem. Soc. Faraday Trans. 2, 78 (1982) 1195- 1209.

Bui, S.H., K.J. McLean, M.R. Cheesman, J.M. Bradley, S.E. Rigby, C.W. Levy, D. Leys, A.W. Munro, J. Biol. Chem. 287 (2012) 19699-19714.

Chen, D. et al. 2005. *Biochem Pharmacol* 69: 1421-1432

Croce, A.C., G. Santamaria, U. De Simone, F. Lucchini, I. Freitas, G. Bottiroli, Photochem. Photobiol. Sci. 10 (2011) 1189-1195

Desagher, S. and J-C. Martinou, Trends Cell Biol. 10 (2000), 369-377

Dooijewaard, G., E.C. Slater, Biochim. Biophys. Acta 440 (1976) 1-15.

Eichler, M., R. Lavi, A. Shainberg, R. Lubart, Lasers Surg. Med. 37 (2005) 314-319.

Felker, P., S. Izawa, N. E. Good, and A. Haug, Biochimica et Biophysica Acta, 325 (1973) 193–196

Fiorani, M., Guidarelli, A., Blasa, M., Azzolini, C., Candiracci, M., Piatti, E., Cantoni, O., 2010.. J. Nutr. Biochem. 21, 397-404.

Floreani, M., Carpenedo, F. 1992. *Gen Pharmacol* 23: 757-762

Foster, K.A., F. Galeffi, F.J. Gerich, D.A. Turner, M. Müller, Progr. Neurobiol. 79 (2006) 136-171.

Gaspers, L.D., A.P. Thomas, , Methods 46 (2008) 224-232.

Goltsev, V., P. Chernev, I. Zaharieva, P. Lambrev, R.J. Strasser, Photosynth. Res. 84 (2005) 209-215.

Gostimskaya, I.S., V.G. Grivennikova, G. Cecchini, A.D. Vinogradov. FEBS Lett. 581 (2007) 5803-5806.

Grivennikova, V.G., E.O. Maklashina, E.V. Gavrikova, A.D. Vinogradov, Biochim. Biophys. Acta 1319 (1997) 223-232.

Guo, Y., J. Tan, BioSystems 95 (2009) 98-103.

Han DW et al. 2011. *Acta Pharmacologica Sinica*, doi: 10.1038/aps.2011.17
Hano, N., Y. Nakashima, K. Shinzawa-Itoh, S. Yoshikawa, J. Bioenerg. Biomembr. 35 (2003) 257-265.
Hatefi, Y., J.S. Rieske, in: R.W. Estabrook, M.E. Pullman (Eds.), Methods in Enzymology, Vol. 10, Academic Press, New York, 1967, pp. 235-239.
Heikal, A.A., Biomark. Med. 4 (2010) 241-263.
Isenberg, J.S., J.E. Klaunig, Toxicol. Sci. 53 (2000) 340-351.
Jeong, J.H. et al. 2009. *J Cell Biochem* 106: 73-82
Johnson MK, Loo G. 2000. *Mutation Res.* 459: 211-218
Ji, H.F., L. Shen, J. Carey, R. Grandori, H.Y. Zhang, J. Mol. Struct. THEOCHEM 764 (2006) 155-160.
Khan, A.U., M. Kasha, J. Am. Chem. Soc. 92 (1970) 3293-3300
Khan, A.U., Activated oxygen: singlet molecular oxygen and superoxide anion. Photochem. Photobiol. 28 (1978) 615-626.
Kindzelskii, A., H.R. Petty, Eur. Biophys. J. 33 (2004) 291-299.
Krause, F., C.Q. Scheckhuber, A. Werner, S. Rexroth, N.H. Reifschneider, N.A. Dencher, H.D. Osiewacz, J. Biol. Chem. 279 (2004) 26453-26461.
Kuznetsov, A.V., O. Mayboroda, D. Kunz, K. Winkler, W. Schubert, J. Cell Biol. 140 (1998) 1091-1099.
Lagoa, R., I. Graziani, C. Lopez-Sanchez, V. Garcia-Martinez, C. Gutierrez-Merino, Biochim. Biophys. Acta 1807 (2011) 1562-1572.
Li, N., K. Ragheb, G. Lawler, J. Sturgis, B. Rajwa, J.A. Melendez, J.P. Robinson, J. Biol. Chem. 278 (2003) 8516-8525.
Liu, M., B. Lei, Q. Ding, J.C. Lee, S.C. Tu, Arch. Biochem. Biophys. 337 (1997) 89-95.
Magnitsky, S., L. Toulokhonova, T. Yano, V.D. Sled, C. Hägerhäll, V.G. Grivennikova, D.S. Burbaev, A.D. Vinogradov, T. Ohnishi, J. Bioenerg. Biomembr. 34 (2002) 193-208.
Marques, I., N.A. Dencher, A. Videira, F. Krause, Eukaryot. Cell 6 (2007) 2391-2405.
Matzno, S. et al. 2008. *Biol Pharm Bull* 31: 1270-1273
Mayevsky, A., G.G. Rogatsky, Am. J. Physiol. Cell Physiol. 292 (2007) C615-C640.
Mik, E. G., J. Stap, M. Sinaasappel, J. F. Beek, J. A. Aten, T. G. van Leeuwen, C. Ince, Nat. Methods 3 (2006) 939- 945
Mik, E. G., T. Johannes, C. J. Zuurbier, A. Heinen, J. H. P. M. Houben-Weerts, G. M. Balestra, J. Stap, J. F. Beek, C. Ince, Biophys. J. 95 (2008) 3977-3990
C. Mieg, W. P. Mei, and F. A. Popp, in Recent Advances in Biophoton Research and its Applications, F. A. Popp, K. H. Li, and Q. Gu Eds (Word Scientific, 1992) 197–205]
Murray, T.A., R.P. Swenson, Biochemistry 42 (2003) 2307-2316]
Nogués, I., L.A. Campos, J. Sancho, C. Gómez-Moreno, S.G. Mayhew, M. Medina, Biochemistry 43 (2004) 15111-15121.
Ohnishi, S.T., T. Ohnishi, S. Muranaka, H. Fujita, H. Kimura, K. Uemura, K. Yoshida, K. Utsumi, J. Bioenerg. Biomembr. 37 (2005) 1-15.
Pérez-Ruiz, T., C. Martínez-Lozano, A. Sanz, E. Bravo, Electrophoresis 22 (2001) 1170-1174.
Ransac, S., C. Arnarez, J.P. Mazat, The flitting of electrons in complex I: A stochastic approach, Biochim. Biophys. Acta 1797 (2010) 641-648.
Sandoval-Acuña, C., C. Lopez-Alarcón, M.E. Aliaga, H. Speisky, Chem. Biol. Interact. 199 (2012) 18- 28.
Sazanov, L.A., Biochemistry 46 (2007) 2275-2288.
Scordino, A., A. Triglia, F. Musumeci, F. Grasso, Z. Rajfur, J. Photochem. Photobiol. B 32 (1996) 11–17
Scordino, A., F. Musumeci, M. Gulino, L. Lanzanò, S. Tudisco, L. Sui, R. Grasso, A. Triglia, Journal of Physics D – Applied Physics 41 (2008) 155507 (7pp)
Scordino, A., I. Baran, M. Gulino, C. Ganea, R. Grasso, J. H. Niggli, F. Musumeci, Journal of Photochemistry and Photobiology B: Biology 139 , pp. 76-84 (2014)
Shuttleworth, C.W., Neurochem Int. 56 (2010) 379-386.
Skog, S., B. Tribukait, B. Wallström, S. Eriksson, Cancer Res. 47 (1987) 6490-6493.
Stroh, A., O. Anderka, K. Pfeiffer, T. Yagi, M. Finel, B. Ludwig, H. Schägger, J. Biol. Chem. 279 (2004) 5000-5007.
Suzuki, H., T.E. King, J. Biol. Chem. 258 (1983) 352-358.

Swartz, T.E., S.B. Corchnoy, J.M. Christie, J.W. Lewis, I. Szundi, W.R. Briggs, R.A. Bogomolni, J. Biol. Chem. 276 (2001) 36493-36500.
Tudisco, S., F. Musumeci , A. Scordino, G. Privitera, Review of Scientific Instruments 74 (2003) 4485- 4490
Tudisco, S., A. Scordino, G. Privitera, I. Baran, F. Musumeci, Nuclear Instruments & Methods in Physics Research A 518 (2004) 463-464
Verkhovskaya, M.L., N. Belevich, L. Euro, M. Wikström, M.I. Verkhovsky, Proc. Natl. Acad. Sci. U.S.A. 105 (2008) 3763-3767.
Villette, S., S. Pigaglio-Deshayes, C. Vever-Bizet, P. Validire, G. Bourg-Heckly, Photochem. Photobiol. Sci. 5 (2006) 483-492.
Vinnakota, K.C., J.B. Bassingthwaighte, Am. J. Physiol. Heart Circ. Physiol. 286 (2004) H1742-1749.
Vinogradov, A.D., Biochim. Biophys. Acta 1777 (2008) 729-734.
Zakharova, N.V., T.V. Zharova, A.D. Vinogradov, FEBS Lett. 444 (1999) 211-216.
Xu, X., E.A. Arriaga, Free Rad. Biol. Med. 46 (2009) 905-913.
Yamaguchi, M., G.I. Belogrudov, A. Matsuno-Yagi, Y. Hatefi, Eur. J. Biochem. 267 (2000) 329-336
Yen, G.C. et al. 2003. *Biosci Biotechnol Biochem* 67: 1215
Yin, W., X. Li, S. Feng, W. Cheng, B. Tang, Y.L. Shi, Z.C. Hua. Biochem. Pharmacol. 78 (2009) 191-202.

7. Dissemination

Articles

1. Ioana Teodora Tofolean, Constanta Ganea, Diana Ionescu, Alexandru Filippi, Alexandru Garaiman, Alexandru Goicea, Mihnea-Alexandru Gaman, Alexandru Dimancea, Irina Baran, Cellular determinants involving mitochondrial dysfunction, oxidative stress and apoptosis correlate with the synergic cytotoxicity of epigallocatechin-3-gallate and menadione in human leukemia Jurkat T cells, ***Pharmacological Research***, in press, 2015 **(if. 4.408)(is.1.170) (ISI))**
2. I. Baran, A. Scordino, D. Ionescu, S. Privitera, R. Grasso, M. Gulino, F. Musumeci, I.T. Tofolean, C. Ganea, Functional characterization of mitochondrial respiratory complex I by delayed luminescence spectroscopy, *LNS Activity Report 2015* Istituto Nazionale Di Fisica Nucleare Laboratori Nazionali Del Sud, 2015; Edit. Marchese Arti Grafiche, Siracusa, Italia; ISSN: 1827-1561 **(BDI)**
3. A. Iftime, C. Ganea**,** A. Popescu Rightmire, Interference of coumarin with the insertion of lyotropic anions and cadmium in artificial lipid bilayers, ***Romanian Biotechnological Letters*****,** Vol. 20, No. 4, Pages: 10637-10647 Published: JUL-AUG 20152015 **(if. 0.404)(is 0.442) (ISI)**
4. Agata Scordino, Irina Baran, Marisa Gulino, Constanta Ganea, Rosaria Grasso, J. Hugo Niggli,Francesco Musumeci, Ultra-weak Delayed Luminescence in cancer research: A review of the results by the ARETUSA equipment, ***Journal of Photochemistry and Photobiology B: Biology*** 139 , pp. 76-84 (2014)**(IF 2.803) (is. 0.843) (ISI)**

Conferences

1. Valentin Popescu, Bogdan Mastalier, Irina Baran. Polycaprolactone microspheres loaded with bioflavonoids and menadione mixture, novel systemic-friendly approach on cancer. Oral presentaion accepted at the international workshop „Electroporation based Technologies and Treatments" European Society for Biomaterials, Ljubljana, Slovenia, 15-21 nov. 2015
2. Roxana Gabriela Sandu, Ioana Teodora Tofolean, Constanta Ganea, Irina Baran. Enhancement of the antiproliferative effect of doxorubicin by quercetin-menadione combinations in human leukemia Jurkat cells. Poster, 6th EMBO (European Molecular Biology Organization) Meeting, 5-8 sept. 2015, Birmingham, England

3. Alexandru Garaiman, Ioana Teodora Tofolean, Irina Baran. Chemotherapeutic potential of combination EGCG:MD in human leukemia Jurkat T cells. Poster, 5th Lower Saxony International Summer Academy in Immunology, 16 august – 13 september 2015, Hannover Medical School, Hannover, Germania. Abstract Book pag. 3
4. Oana Elena Baran, Ioana Teodora Tofolean, Ruxandra Irimia, Irina Baran, Constanta Ganea. Antiproliferative effect of doxorubicin/quercetin/menadione combination in leukemia Jurkat T cells. Poster, 10th EBSA European Biophysics Congress, 18-22 July 2015, Dresda, Germania. Late Abstract Booklet p. 44
5. Vlad Cosoreanu, Ioana Teodora Tofolean, Constanta Ganea, Alexandru Goicea, Irina Baran. Growth-suppressive action of doxorubicin on human leukemia Jurkat cells. Modulation by quercetin. Poster, 10th EBSA European Biophysics Congress, 18-22 July 2015, Dresda, Germania. Late Abstract Booklet p. 45
6. Maria Teodora Ilie, Ioana Teodora Tofolean, Constanta Ganea, Alexandru Dimancea, Irina Baran. Chemotherapeutic potential of the doxorubicin/menadione combination in a human leukemia cell model. Poster, 10th EBSA European Biophysics Congress, 18-22 July 2015, Dresda, Germania. Late Abstract Booklet p. 45
7. Valentin Popescu, Bogdan Mastalier, Irina Baran. Bioflavonoids and menadione potential in novel systemic-friendly approach on cancer. Poster at the international workshop „YOUNG SCIENTISTS JOINING FORCES FOR EXCELLENCE IN BIOMATERIALS RESEARCH" European Society for Biomaterials, Bucureşti, 28-29 mai 2015. **Prize „Best Poster Award"**
8. Ruxandra Irimia, Irina Baran. Green tea derived EGCG and vitamin K3: a synergic antiproliferative effect in acute lymphoblastic leukemia. MEDICALIS International Congress for Medical Students and Young Professionals, 14-17 May 2015, Cluj-Napoca
9. Paul Ciucur, Simona Costache, Irina Baran, Constantea Ganea. Possible therapeutic attitude towards acute lymphoblastic leukemia. MEDICALIS International Congress for Medical Students and Young Professionals, 14-17 May 2015, Cluj-Napoca
10. Simona Costache, Paul Ciucur, Alexandru Filippi, Irina Baran. Modularea efectului antitumoral al doxorubicinei asupra celulelor umane leucemice Jurkat cu combinații quercetină-menadionă. Comunicare orală, Congresul Naţional pentru Studenţi şi Tineri Medici, Bucureşti, martie 2015. **Ist Prize**. Abstract booklet ISSN 2285-9438
11. A. Filippi, T. Picot, C.M. Aanei, L. Campos, C. Ganea, M.M. Mocanu, Epigallocatechin-3-O-gallate reduces the clonogenicity, induces the mitochondrial depolarization and increases production of reactive oxygen species in cancer cell lines with ErbB proteins overexpression, International Conference of the Romanian Society of Biochemistry and Molecular Biology, Bucharest, 17-18 September 2015, ISBN 978-973-720-605-3
12. M.M. Mocanu, A. Filippi, T. Picot, C. M. Aanei, L. Campos, C. Ganea, Anticancer effects of epigallocatechin-3-*O*-gallate in tumor cell lines with ErbB proteins overexpression, poster, National Conference of Cytometry, May 20, 2015, Bucharest, Romania